AD-A088 732 HUGHES RESEARCH LABS MALIBU CA F/6 17/5
SILICON-GERMANIUM ALLOYS FOR INFRARED DETECTORS.(U)
APR 80 H WINSTON, H KIMURA, R BARON F33615-77-C-5052
UNCLASSIFIED AFWAL-TR-80-4031 NL

1 OF 1
AD
A088732

END
DATE
FILMED
10-80
DTIC

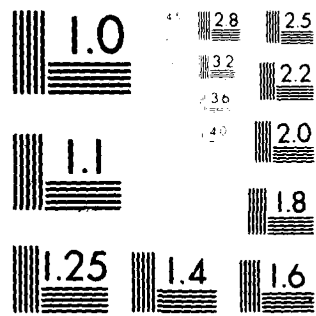

MICROCOPY RESOLUTION TEST CHART
NATIONAL BUREAU

AFWAL–TR–80–4031

AD A088732

SILICON–GERMANIUM ALLOYS FOR INFRARED DETECTORS

H. Winston, H. Kimura R. Baron
Hughes Research Laboratories
3011 Malibu Canyon Road
Malibu, CA 90265

Apr 80

Technical Report AFWAL–TR–80–4031
Final Report, 15 Aug 77 – 14 Aug 79

Approved for public release; distribution unlimited

SEP 4 1980

A

MATERIALS LABORATORY
AIR FORCE SYSTEMS COMMAND
UNITED STATES AIR FORCE
Wright–Patterson AFB, OH 45433

DDC FILE COPY

80 9 2 158

NOTICE

When Government drawings, specifications or other data are used for any purpose other than in connection with a definitely related Government procurement operation, the United States Government thereby incurs no responsibility nor any obligation whatsoever; and the fact that the government may have formulated, furnished, or in any way supplied the said drawings, specifications, or other data, is not to be regarded by implication or otherwise as in any manner licensing the holder or nay other person or corporation, or conveying any rights or permission to manufacture, use, or sell any patented invention that may in any way be related thereto.

This report has been reviewed by the Office of Public Affairs (ASD/PA) and is releasable to the National Technical Information Service (NTIS). At NTIS, it will be available to the general public, including foreign nations.

This technical report has been reviewed and is approved for publication.

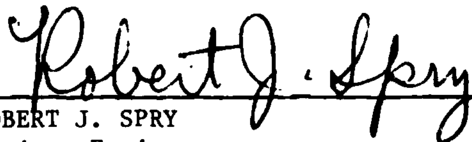

ROBERT J. SPRY
Project Engineer

G. EDWARD KUHL, Chief
Laser & Optical Materials Branch
Electromagnetic Materials Division

FOR THE COMMANDER

MERRILL L. MINGES, Chief
Electromagnetic Materials Division
Materials Laboratory
Air Force Wright Aeronautical Laboratories

"If your address has changed, if you wish to be removed from our mailing list, or if the addressee is no longer employed by your organization please notify AFWAL/MLPO, W-PAFB, OH 45433 to help us maintain a currect mailing list".

Copies of the report should not be returned unless return is required by security considerations, contractual obligations, or notice on a specific document.

AD-A088732

SECURITY CLASSIFICATION OF THIS PAGE (When Data Entered)

REPORT DOCUMENTATION PAGE

READ INSTRUCTIONS BEFORE COMPLETING FORM

Field	Entry
1. REPORT NUMBER	AFWAL/-TR-80-4031
2. GOVT ACCESSION NO.	AD-A088732
3. RECIPIENT'S CATALOG NUMBER	
4. TITLE (and Subtitle)	SILICON-GERMANIUM ALLOYS FOR INFRARED DETECTORS
5. TYPE OF REPORT & PERIOD COVERED	Final Report 15 Aug 1977 - 14 Aug 1979
6. PERFORMING ORG. REPORT NUMBER	
7. AUTHOR(s)	H. Winston, H. Kimura, and R. Baron
8. CONTRACT OR GRANT NUMBER(s)	F33615-77-C-5052
9. PERFORMING ORGANIZATION NAME AND ADDRESS	Hughes Research Laboratories 3011 Malibu Canyon Road Malibu, CA 90265
10. PROGRAM ELEMENT, PROJECT, TASK AREA & WORK UNIT NUMBERS	Project No. 2306Q101
11. CONTROLLING OFFICE NAME AND ADDRESS	Materials Laboratory Air Force Wright Aeronautical Laboratories (AFWAL/MLPO) Wright-Patterson AFB, OH 45433
12. REPORT DATE	April 1980
13. NUMBER OF PAGES	67
14. MONITORING AGENCY NAME & ADDRESS (if different from Controlling Office)	
15. SECURITY CLASS. (of this report)	
15a. DECLASSIFICATION/DOWNGRADING SCHEDULE	

16. DISTRIBUTION STATEMENT (of this Report)

Approved for public release; distribution unlimited.

17. DISTRIBUTION STATEMENT (of the abstract entered in Block 20, if different from Report)

18. SUPPLEMENTARY NOTES

19. KEY WORDS (Continue on reverse side if necessary and identify by block number)

Silicon-germanium alloys, Czochrolski growth, crucible-free growth, Hall-effect analysis, site effect on impurity levels.

20. ABSTRACT (Continue on reverse side if necessary and identify by block number)

Silicon-germanium alloys in the range of 10 at.% Ge have been prepared by Czochralski growth. Material that was not intentionally doped exhibited resistivities as high as 1700 Ω-cm, but, because of the uptake of boron impurities from the crucible during growth, higher resistivities could not be achieved. Therefore, even though the alloys had absorption coefficients for 1.06 μm radiation around 50 cm^{-1} (in contrast to 14 cm^{-1} for silicon), they were not well suited to preparing p-i-n detectors for 1.06 μm applications because the -

DD FORM 1473, 1 JAN 73 EDITION OF 1 NOV 65 IS OBSOLETE

SECURITY CLASSIFICATION OF THIS PAGE (When Data Entered)

resistivities were too low to provide suitable long depletion regions. We prepared some alloy crystals by a crucible-free process (which would lead to high resistivity) akin to float zoning. The maximum Ge content achieved was about 2.5 at.%; while this value could be increased by equipment modification and process development, a fundamental drawback of the method is an axial variation of the germanium content as the germanium initially present in the zone is depleted.

Measurements of minority carrier diffusion lengths in device structure made of p-type Si-Ge and of p-type Si showed essentially equivalent recombination lifetimes for both materials as processed to make the devices; the lifetime values were close to 100 nsec. At room temperature, the mobility in p-type Si-Ge is degraded by 10 to 20% from the Si value. At cryogenic temperature, the mobility reduction is much larger, but is consistent with the disorder scattering estimated from room temperature measurements.

Careful Hall measurements on nominally undoped and indium-doped Si-Ge reveal the presence of several energy levels for each of the acceptors B and In. The major factor in determining the value of the energy level is the local environment of the acceptor, that is, the number of germanium nearest neighbors. Among the In levels is one at 0.107 eV associated with a site having one Ge and three Si neighbors in $Si_{0.89}Ge_{0.11}$. This level is interesting for the 8- to 12-μm spectral region, but it is associated with a larger density of deeper levels on In atoms with four Si neighbors.

PREFACE

The following people have contributed significantly to the work reported here: C. Afable, P. Amini, J.P. Baukus, W.P. Fleming, M.F. Harvey, J.A. Henige, O.J. Marsh, K.T. Miller, D.J. O'Connor, A.F. Rabideau, A.J. Timper, S. Turley, R. Wong-Quen, and M.H. Young. The report was written by H. Winston, H. Kimura, and R. Baron.

TABLE OF CONTENTS

SECTION		PAGE
	LIST OF ILLUSTRATIONS	7
	LIST OF TABLES	9
1	INTRODUCTION	11
2	CZOCHRALSKI GROWTH	15
3	CRUCIBLE-FREE GROWTH	23
4	MEASUREMENTS OF COMPOSITION	27
5	X-RAY-DIFFRACTION STUDIES OF Si-Ge ALLOYS	29
6	OPTICAL AND ELECTRICAL MEASUREMENTS	31
	A. Infrared Absorption Measurements	31
	B. Hall Analysis	31
	C. Near-Infrared Spectral Response Measurements	54
	D. Minority-Carrier Diffusion Length	54
	E. Spectral Response	59
7	CONCLUSIONS AND RECOMMENDATIONS	61
	REFERENCES	63

LIST OF ILLUSTRATIONS

FIGURE		PAGE
1	Heater assembly for NRC crystal puller	17
2	Acceptor concentration of Si-Ge and Si crystals	20
3	Crucible-free growth of Si-Ge crystals	24
4	X-ray topograph of Si-Ge crystal, showing rotational striations caused by small variations in composition	30
5	Dependence of absorption coefficient on photon energy at 292°K for Si-Ge alloys and Si	32
6	Shift in band edge ($\alpha = 36\ cm^{-1}$) versus composition	33
7	Carrier concentration versus temperature for Si:Ge:B showing explicit appearance of both of the observed energy levels depending on the degree of composition	36
8	Carrier concentration versus temperature for Si:Ge:B	40
9	Carrier concentration versus temperature for Si:Ge:In showing the extent to which the data is dominated by undercompensated residual B	44
10	Observed ionization energies versus x in $Si_{(1-x)}Ge_x$	48
11	Mobility versus temperature for a number of Si:Ge and Si samples	49
12	Mobility versus temperature for a number of In-doped Si:Ge and Si samples	50
13	Comparison of disorder induced scattering lifetimes in Si:Ge	52
14	Comparison of $\mu_{disorder}$ versus X in $Si_{(1-x)}$ Ge_x to the theoretical expected shape	53

FIGURE PAGE

15 Photocurrent versus depletion layer width for Si:Ge $p^+\pi n^+$ structure 57

16 Photocurrent versus depletion layer width for Si $p^+\pi n^+$ structure 58

17 Relative photocurrent versus wavelength for Si and Si:Ge $p^+\pi n^+$ structures 60

LIST OF TABLES

TABLE		PAGE
1	Crystal Growth Conditions	16
2	Comparison of Percent Ge Determined by Electron Microprobe, Density, and X-Ray (Powder) Methods . .	28
3	Si:Ge Hall Analysis Results	37
4	Analysis of Hall Data for C093In.61 Assuming One or Two Levels for Boron	39
5	Probability of a B Site in $Si_{(1-x)}Ge_x$:B Having k Ge Nearest Neighbors	42
6	Analysis of Hall Data for C110In.T6	45

SECTION 1

INTRODUCTION

The prospective applications of Si-Ge alloy materials to intrinsic and extrinsic photodetectors imply a list of goals for a research program on the preparation and characterization of these materials. One crucial issue is the possibility of preparing the alloys in highly perfect single-crystal form as ingots of 1-in. or 2-in. diameter. This is necessary because the silicon device technology we expect to extend to the alloy is based on large-diameter single-crystal wafers. Typical intrinsic Si detectors are fabricated from high-resistivity single-crystal 1-in. wafers, and the processes for infrared-sensitive monolithic focal plane arrays (MFPAs) begin with intentionally doped single-crystal wafers at least 2 in. in diameter. A second essential issue relates to the control and uniformity of alloy composition, both radially and axially, in the ingot. Since the virtue of using an alloy is the possibility of adjusting its optical and electronic properties by the choice of composition, it is important to be able to prepare alloy crystals of a definite and controllable composition. The third major requirement is that Si-Ge alloys must be prepared, just as in the case of Si, without significant contamination by unintentional impurities. Electrically active impurities must be kept at or below the 10^{12} cm^{-3} range. Thus, our work on the growth of Si-Ge alloys has been guided by the requirements of

- Crystallinity (good crystals up to 1 or 2 in. in diameter)
- Compositional control and uniformity
- High purity.

We reported progress in the first year of this two-year program in an interim report[1] issued in February 1979. That report is summarized here to set the stage for the second year's work, reported in detail in the following sections. Our major effort during the first year was in growing Si-Ge of about 10 at.% Ge content without intentional doping.

To avoid extreme lattice mismatch between seed and crystal, we originally intended to follow a program strategy in which a series of seeds of increasing Ge content would be prepared by Czochralski growth from Si-Ge melts with increasingly higher Ge contents. Starting with a pure Si seed and a low-Ge melt, a crystal containing some Ge can be obtained that could serve as a seed in the next growth from a higher Ge melt, and so on, until a crystal of the desired Ge content is obtained. Although we expected that the purity of such a crystal would not be particularly high, because impurities would build up from the interaction of the melt with the crucible required in Czochralski growth, we felt that it could be cut up into seeds to be used in some form of crucible-free growth of Si-Ge of the desired composition. But we did not actually carry out this strategy for three reasons:

- The growth rate necessary to obtain reasonably good Si-Ge crystals is very low, on the order of millimeters per hour (or less) rather than millimeters per minute as in the Czochralski growth of lightly doped Si. This made the individual growth runs very time consuming and the overall sequence of increasing Ge concentrations prohibitively lengthy. We decided to try to reduce the time required by using fewer steps, each with a larger change in Ge content. In fact, in our first attempts, we grew 6 to 7 at.% Ge alloys directly from Si seeds.

- These 6 to 7 at.% crystals, however, were unsuitable as seeds because they were twinned. They were grown by the conventional method of starting with a narrow seed, adjusting the pull rate and the heater power to make the growing crystal gradually increase in diameter up to the desired value, and then maintaining the diameter constant by a further adjustment of the grower controls. It appeared that twinning might be associated with the transition from the seed to a larger diameter: twinning is sometimes encountered at this stage in the growth of Si crystals, and the tendency might well be accentuated under the very slow growth rates needed for Si-Ge. To avoid carrying out the diameter transition in high-Ge material, we grew a Si-Ge shoulder of 0.6 at.% Ge out to diameter and then used the shoulder as a seed in a high-Ge melt to obtain single-crystal Si-Ge close to the desired 10 at.% Ge content. Subsequently, we found that it is possible to start with a 100 at.% Si shoulder and achieve the desired Si-Ge alloy directly.

- Since some of the Si-Ge prepared in this way exhibited high resistivity, we decided to investigate the possibility of using high-purity crucibles to obtain Si-Ge suitable for 1.06-μm detector purposes, instead of resorting to crucible-free growth. Czochralski growth seemed particularly attractive because we expected it to be the only growth method suitable for preparing In-doped Si-Ge for longer wavelength infrared detector applications. Since we would have to control purity in the growth of doped Si-Ge from crucibles in any event, we hoped that the same approach could be applied to preparing undoped, high-resistivity Si-Ge.

Thus, we had found a way to grow ∿10 at.% Si-Ge directly from the melt in one step using a Si shoulder of the desired final diameter as the seed. The remaining difficulty was to reduce contamination by impurities entering the melt as the melt etched the crucible; we investigated the use of high-purity synthetic quartz as a crucible liner. Our experiments with these crucible liners were complicated by the growth of bubbles in the liner material during long growth runs. These bubbles caused the melt level to rise faster than the withdrawal rate of the seed. On the hypothesis that the bubbles were caused by water vapor deriving from the hydroxide ions in which synthetic quartz is rich, we adopted a bakeout process to reduce the hydroxyl content. The synthetic-quartz-lined crucible was baked out in vacuum at 1300°C for 16 hr followed by 4 hr at 1420°C before being used for a crystal growth run. By this method, we obtained a $Si_{0.89}Ge_{0.11}$ crystal (C077Ge) containing, after heat treatment to eliminate the oxygen donors present in the as-grown condition, a net boron concentration (boron minus donors) of $\sim 10^{13}$ cm^{-3} and a total boron concentration no higher than the mid-10^{13} range. This material also exhibited approximately the expected change in band-edge absorption.

At the end of the first year, therefore, we had evidence that there is a set of growth conditions that will result in an undoped crystal of relatively high purity. Our plan for the second year was to explore the possibilities of further reducing the boron content in undoped Si-Ge, and to prepare indium-doped crystals (also with low boron content) suitable for extrinsic detector applications.

In the work described in this report, we made progress towards each of these goals, but we also encountered obstacles that prevented

complete success. Although we were not able to define growth procedures having the promise of producing device-quality meterial in any satisfactory yield, we were able to gain a better understanding of impurity levels in the Si-Ge alloy and to confirm the basic principle of shifting the intrinsic energy gap and extrinsic energy levels by changes in alloy composition.

SECTION 2

CZOCHRALSKI GROWTH

Crystal C087Ge, the last crystal grown during the first year of the program, grew largely single, although with some obvious twins and other crystal defects. The as-grown resistivity ranged from 500 to 6000 Ω-cm p-type. We decided to grow several more undoped crystals, aiming at improved crystallinity and higher resistivity and to extend the Czochralski growth method to indium-doped Si-Ge alloys. Our intention was to select the best samples for further detailed analysis by Hall-effect measurements. The crystals grown during the second year of the program are listed in Table 1.

C089Ge was grown under vacuum with growth conditions similar to those of previous crystals. It was polycrystalline but with large enough grains to make Hall measurements. The boron concentration from Hall analysis was in the mid-10^{13} cm^{-3} range, similar to our best previous results. Figure 1 shows the heater assembly of the crystal puller used in this and later growth runs. In some runs the molybdenum heat shield was replaced by graphite felt. The quartz crucible (not shown) fits inside the graphite crucible cup.

C091Ge was grown under conditions identical to those for C089Ge. It was 100% single and had a room-temperature resistivity of 330 to 350 Ω-cm p-type, suggesting a boron concentration at or above the mid-10^{13} cm^{-3} range.

C092Ge started as an attempt to increase purity by using a new heater assembly, along with a 4-in.-diameter Suprasil crucible, in vacuum. The Hall measurement showed that the boron concentration was in the high-10^{14} cm^{-3} range, more than an order of magnitude higher than in crystal C089Ge. Apparently, the new heater increased rather than lowered the boron impurity.

Table 1. Crystal Growth Conditions

Crystal Number	Melt Weight, g	Melt Composition	Composition	Growth Rate, mm/hr	Seed Rotation, rpm	Crucible Rotation Rate, rpm	Ambient Gas	Orientation	Crystal Length, mm	Crystal Diameter, mm	Crystallinity	Ge Source	Crucible	Comments
C089	300	Si 0.72 Ge 0.28		0.5	10	18	Vac	<111>	15	22 to 40	Poly	Ortec		
C091	300	Si 0.72 Ge 0.28		0.5	10	18	Vac	<111>	5 to 7	29 (max)	Single	Ortec	Suprasil, heat treated	
C092	285	Si 0.72 Ge 0.28		0.5	10	20	Vac	<111>	7	22 (max)	Single	Ortec	Suprasil, heat treated	
C093 In	360	Si 0.72 Ge 0.28	Ge 10.9 Si 88.1	0.5	8	10	Vac	<111>	8 to 9	10		Ortec	Suprasil, heat treated	Graphite felt
C097	200	Si 1.00		64	6	8	He 70 Torr	<100>	100	20	Single		Quartz	Molybdenum heat shield, Vitre-Graf heater assembly
C098	240	Si 1.00		50	6	8	He 50 Torr	<100>	140	20	Single		Suprasil, heat treated	Vitre-Graf heater, molybdenum heat shield
C106	240	Si 1.00		50	9	6	He 800 Torr	<100>	100	20				
C107	240	Si 0.78 Ge 0.22	Ge 8.3-8.8 Si 91.7	0.5	8	6	He 800 Torr	<111>	5	25		Ortec	Suprasil, heat treated	Vitre-Graf heater assembly, molybdenum heat shield
C108	300	Si 0.72 Ge 0.28	Ge 11.3 Si 88.7	0.5	8	6	He 800 Torr	<111>	2	27	Single	Ortec	Suprasil, heat treated	Vitre-Graf coated cup with molybdenum liner molybdenum heat shield
C109	287	Si 0.71 Ge 0.29		0.5	9	6	He 800 Torr	<111>	22	25 (max)	Single	Ortec	Suprasil, heat treated	Tantalum strip between the crucible and the graphite holder
C110 In	300	Si 0.72 Ge 0.28		0.8-2.5	10	6	He 800 Torr	<111>	9	26	Single	Ortec	Suprasil, heat treated	In 4.79g, phosphorus DOPE-SIL 25 x 10^{16} atoms
Z157		Si 0.96 Ge 0.04		76	0[a]	2[b]	Ar	<100>	280	15	Single	Ortec		
Z161		Si 0.88 Ge 0.12		64	2	2	Ar	<100>	42	22	Single	Ortec		
Z166		Si 0.83 Ge 0.17		64	1	0	Ar	<100>	150	20	Single	Ortec		

[a] Lower rod rotation rate

[b] Upper rod rotation rate

6955

9859 1

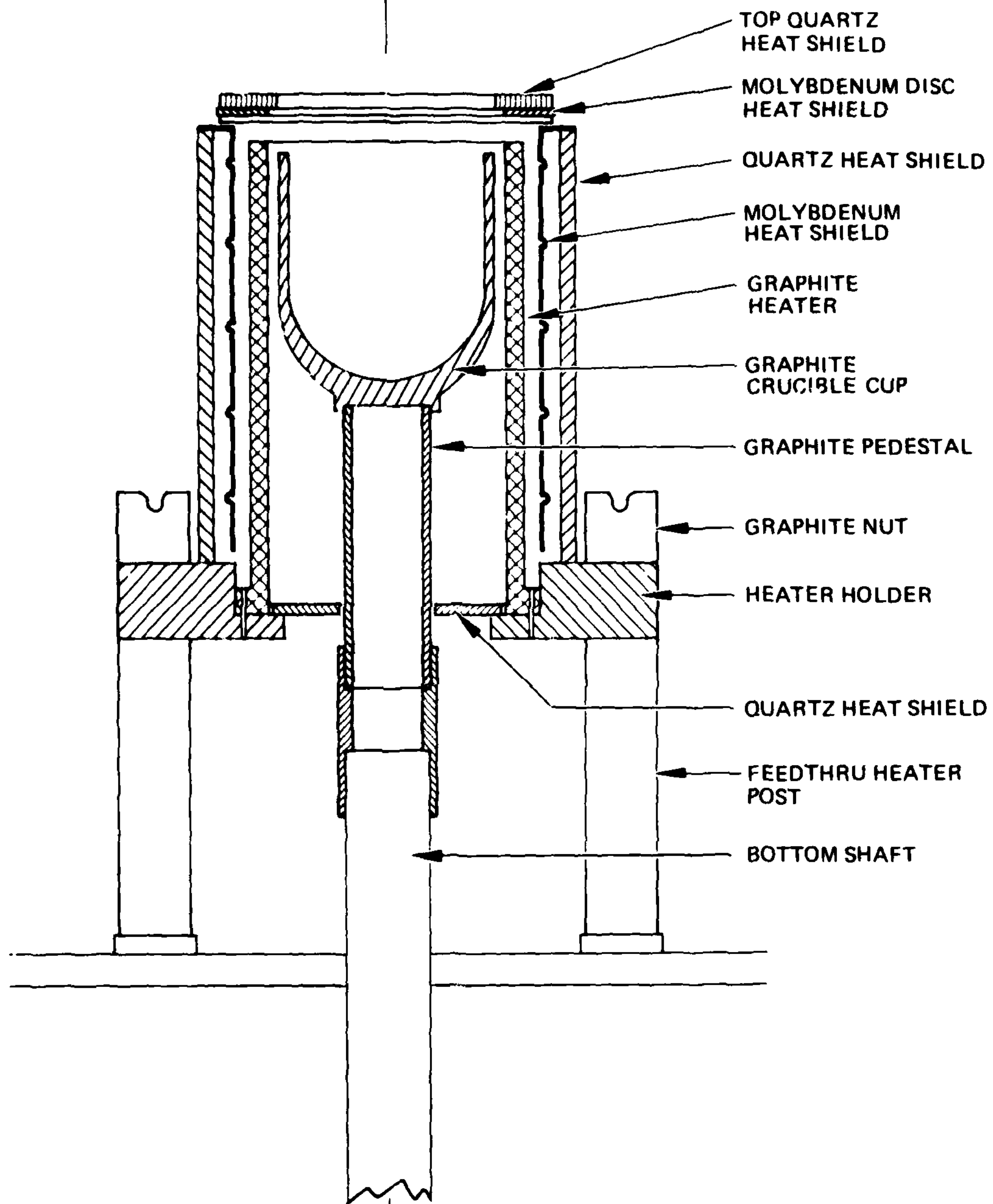

Figure 1. Heater assembly for NRC crystal puller.

Since it was important to have indium-doped material to study, our next crystal was C093Ge:In. Seeking to avoid the problems of the new heater, we used an old heater that had previously been used in growing In-doped Si. Crystal C093Ge:In was grown under 50 Torr He pressure using a Suprasil crucible. But to our dismay, the boron concentration turned out to be above 10^{15} cm^{-3}, much higher than our best previous result and of course far too high for "intrinsic" applications such as 1.06-μm detectors.

With the boron concentration seriously out of control, we planned a series of pure silicon crystal growth runs to examine the sources of contamination. C096 was a pure Si crystal grown with a Vitre-Graf heater. This heater is made by applying a vitreous C coating to a prepurified graphite heater. Since that coating is of high purity and is much less porous than is the regular graphite heater, the transport of C and other impurities into the melt is reduced. The actual crystal growth was not too successful because the graphite felt, which had been used previously as a heat shield in the growth furnace, was removed as a possible contamination source. But removing the heat shield made it necessary to run the heater at a much higher temperature, causing some breakdown of the Vitre-Graf coating and the transport of C to the melt. This crystal was not analyzed for B concentration.

Another pure Si crystal, C097, was grown using the same Vitre-Graf heater assembly but with a Mo heat shield. The crystal was grown in a regular quartz crucible and had a net acceptor concentration of 3.8 x 10^{14} cm^{-3}. Finally, we grew another pure Si crystal, C098, under the exact conditions used for C097 with the exception that a Suprasil crucible was used instead of regular quartz. The use of the high-purity crucible reduced the net acceptor concentration to 5.3 x 10^{13} cm^{-3}, an encouraging improvement. Several growth attempts subsequent to C098 suffered from SiC scum formation on the surface of the melt. The combination of a deteriorated Vitre-Graf heater assembly and growth under partial vacuum enhanced the transport of C to the melt.

A good Si crystal, C106, was grown by using the same Vitre-Graf assembly, applying a slight overpressure of He, and using a Suprasil crucible. The net acceptor concentration at the tang end was 1.6×10^{13} cm^{-3}.

With this encouraging result from C106, we returned to alloy growth. C107Ge and C108Ge were grown under the same conditions as C106 had been, except that the growth rate was 0.5 mm/hr rather than 5 cm/hr; C109Ge was pulled at 2.5 mm/hr to see if a shorter growth time would lead to a lower boron concentration. The melt of C107Ge was contaminated by a speck of impurity that fell from the pull rod into the melt. No Hall measurement was made on C108Ge; its unannealed room-temperature resistivity, however, was about 500 Ω-cm. For C109Ge, Hall measurements gave an acceptor concentration at the tang (an upper limit to the boron concentration) that was about the same as for the C089Ge, which grew at 0.5 mm/hr. Although it was gratifying to be able to produce a crystal in the mid-10^{13} cm^{-3} range of boron concentration, it was disconcerting that C109Ge, grown with a Vitre-Graf heater, a Mo heat shield, and a Ta insert between the crucible holder and the Suprasil crucible, was not clearly superior to C089Ge, grown with a regular heater, a graphite felt heat shield, and a regular quartz crucible.

The last crystal grown in the program was C110Ge:In. The growth conditions were similar to those for C109Ge except that a phosphorus Dopsil pellet was added to the melt in an attempt to overcompensate the boron and thus avoid boron domination of the detector's behavior at low temperatures. The amount of phosphorus added was not quite enough to overcompensate; however, the concentrations of P and B did allow Hall-effect determination, as discussed below. The boron concentration turned out to be in the mid-10^{14} cm^{-3} range.

The acceptor concentrations of Si and Si-Ge crystals are plotted in Figure 2, with the various furnace parts used to grow the crystals listed, in an attempt to determine the source(s) of the excess acceptor. We cannot fully explain the reasons for all the variations in boron concentration. We can, however, make some observations about the influence of certain process changes:

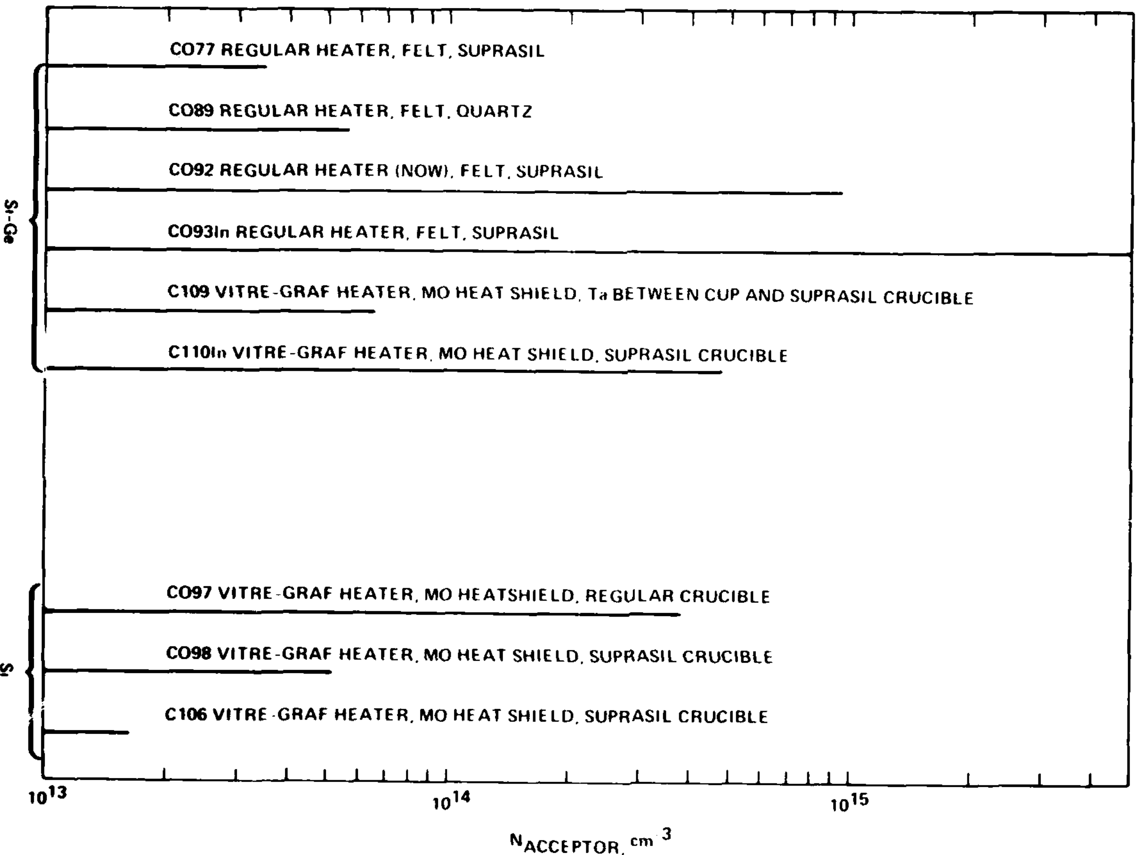

Figure 2. Acceptor concentration of Si-Ge and Si crystals.

- Variations in heater purity are sufficient to cause more than an order of magnitude increase in acceptor concentration. (Cf. C092.)

- Using a refractory metal liner between the crucible and the graphite crucible holder reduces the degradation of crucible holder and crucible via the reduction of silica by carbon to form carbon monoxide and silicon monoxide; impurities volatilized by this degradation may contaminate the melt. (Cf. C097 and C098.)

- Increasing the overpressure reduces the transport of C and the acceptor into the melt. C098 and C106 were grown at 50 and 800 Torr, respectively.

- When other sources of contamination are under control, using Suprasil crucibles is helpful. Although the purity of both regular and Suprasil crucibles varies from batch to batch, Suprasil is generally about an order of magnitude purer in boron.

SECTION 3

CRUCIBLE-FREE GROWTH

Because of the disappointingly high boron concentrations achieved in Czochralski growth, we decided to explore a crucible-free method for preparing Si-Ge alloys. The original idea was to use a form of pedestal growth: Ge would be melted on the top of a Si pedestal to form an alloy melt contained within unmelted Si, and a crystal would then be pulled from the melt by introducing a seed and withdrawing it. In this simple form, the idea has many practical drawbacks associated with heating methods and temperature control. Although we lacked suitable equipment for applying the method directly, we did have a float-zone growth system, which we were able to use to grow Si-Ge alloy material by what might be considered a cross between pedestal and float-zone growth.

Briefly put, this hybrid method consisted of sandwiching Ge between upper and lower Si rods, applying power through an rf coil to generate a molten zone of Si-Ge alloy between these rods, and then moving the rods so that the molten zone passed through them, leaving a solid Si-Ge alloy crystal region behind. The method is outlined in Figure 3 and detailed below.

In Step 1, a single-crystal Si rod (oriented [100] in our work) is held by molybdenum fingers in the normal seed position. A molybdenum susceptor around the fingers is heated by the rf coil and eventually heats the Si rod; the rf power is kept low enough to avoid melting of the Si skin. The rod is long enough so that a quantity of Ge placed on its top does not melt at this point.

In Step 2, the Si rod is lowered slowly through the rf coil; the heated region of the Si moves relative to the rod, but stays fixed with respect to the rf coil. At the end of Step 2, the Ge at the top of the rod is positioned in the center of the rf coil. Then in Step 3, a Si-Ge melt is formed at the top of the Si rod.

In Step 4, another Si rod is lowered onto the Si-Ge melt, sandwiching the melt between the two Si rods. In Step 5, the upper rod becomes hot. When the two rods are first pushed together, they rotate as a

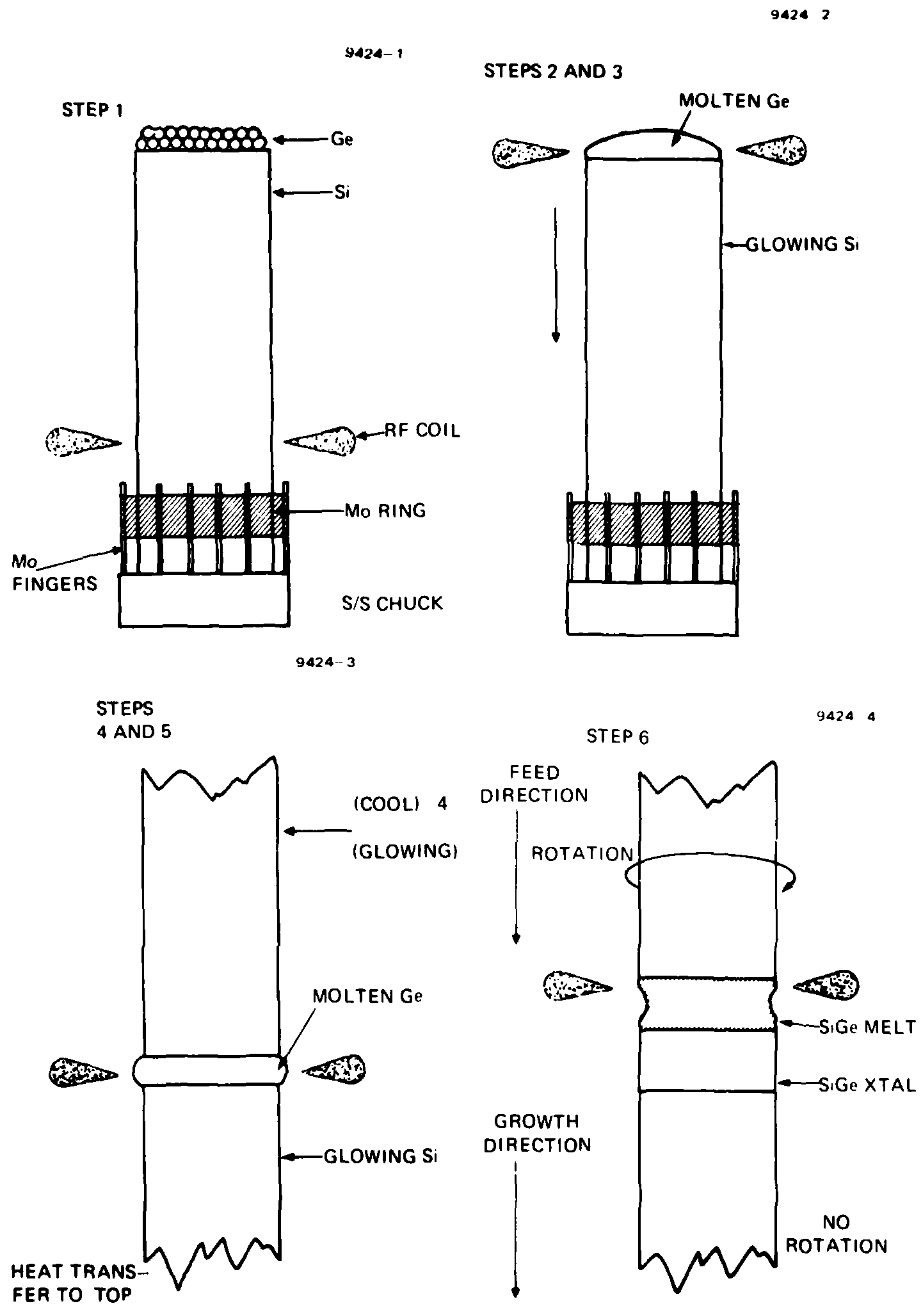

Figure 3. Crucible-free growth of Si-Ge crystals.

unit; but when the zone is completely melted through, the upper rod can be rotated without transferring the rotation to the lower rod. At this point, there exists a zone of liquid Si-Ge alloy, and growth of solid alloy proceeds (in Step 6) in the normal float-zone procedure. With the upper rod rotating, both upper and lower rods are translated vertically downward through the rf coil, resulting in the growth of Si-Ge solid on the lower rod.

We did produce Si-Ge alloy crystals by this technique, but the material was not satisfactory for the application envisioned in this program. Although the original high resistivity of the Si rods could be maintained, indicating freedom from contamination, the composition of the alloy changed along the axis of the crystal. This was the result of depletion of the finite amount of Ge originally introduced. Even the highest Ge concentration attained was much less than 10%.* This low peak concentration could probably be improved by directly controlling the temperature of the molten zone to maintain a suitably high Ge concentration in the melt; this would require extended equipment design and modification. Finally, the slowest growth rate available in our float-zone apparatus was in the millimeters per minute range; this led to pronounced cellular growth and defective crystallinity. The growth conditions for the crucible-free crystals (denoted by the prefix Z) are listed in Table 1.

---

*The method used for measuring Ge concentration — a lattice constant measurement in a single-crystal diffractometer — is not, as discussed below, very accurate. But the value it produced, 2.5%, is so low that we know the true Ge concentration is far short of 10%.

SECTION 4

MEASUREMENTS OF COMPOSITION

During the first year of the program, we measured the Si and Ge content of Si-Ge alloys using a MAC Model S Series combined electron microprobe analyzer/scanning electron microscope using 15-keV Cu K_{α} radiation for both Si and Ge. The data were analyzed by the MAGIC program to take account of various corrections in the final calculation of composition. During the second year of the program, this instrument was no longer available for composition measurement. However, we had already established the melt conditions required to produce alloy crystals in the 10 to 11 at.% Ge range, and the absence of a convenient technique for measuring composition did not interfere with our work. Nevertheless, toward the end of the program, we had occasion to determine the lattice parameters of some of our later crystals. These lattice parameters, measured on single crystals, seemed to correspond to compositions in the 6 to 7 at.% Ge range, instead of the expected 10 to 11 at.%. Therefore, we made composition measurements by several additional techniques, as described below. These measurements generally confirmed the original electron microprobe measurements and provided reliable values in the 10 to 11 at.% range for the later crystals. (The reasons for the erroneous lower values derived from single-crystal lattice parameter measurements are discussed in Section 5.)

Density was determined by the hydrostatic weighing method employing Archimedes's principle. Polished and unpolished wafers weighing from 0.1 to 2 g were used. For weighing samples in air and water, we employed a Mettler H54 semimicro balance, which is readable to 0.01 mg with a precision of 0.01 mg. The buoyancy was corrected for the surface tension of water, and the density of water was corrected for the temperature. The buoyancy of the sample in air was small and was neglected. Measurements of the density of Si when the sample weight was $\sim$0.3 g were within 0.1% of the literature value. To convert density to percent Ge, we used the average curve drawn through the experimental points by Dismukes, Ekstrom, and Paff.[2]

A possible objection to the density technique is that the crystals may not be homogeneous. The absence of gross inhomogeneities is demonstrated by infrared microscope observation of wafers polished on both sides. Furthermore, when a series of electron microprobe measurements was made across the diameter of a wafer, the results were uniform within about 1 at.%, apparently ruling out large variations in composition within a wafer.

Some samples that were too small to give accurate density results were measured by X-ray powder (rather than single-crystal) techniques.

Table 2 shows the results for several crystals. All three methods give composition values in close agreement for crystal C077, the only one to be subjected to all three determinations. In addition, a Rutherford backscattering determination of the composition of C077 was kindly provided to us by Professor R.R. Hart of Texas A&M University; at 11.3 at.%, it is in excellent agreement with the other methods. Although the cause for the disagreement between electron microprobe and density measurements on C068 is not known, the value of 11.6% determined by the density measurement is favored in view of the melt composition.

Table 2. Comparison of Percent Ge Determined by Electron Microprobe, Density, and X-Ray (Powder) Methods

Crystal	Electron Microprobe	Density	X-Ray
C021-3	6.77	6.85	
C021-6	6.82	6.83	
C068	9.05	11.6	
C074	10.77	10.9	
C077	11.15	11.3	11.3
C093			10.4
C107		8.3 to 8.8[a]	
C108		11.3	
C110			10.9

[a]Axial variations.

6955

SECTION 5

X-RAY-DIFFRACTION STUDIES OF Si-Ge ALLOYS

We have used X-ray-diffraction methods to determine the lattice constants, and thus the composition, of Si-Ge alloys, and have also made X-ray topographs to assess the crystal perfection of some samples.

Although lattice constant measurements on single crystals can be highly precise, our measurements led to values of composition that conflicted with those obtained by other methods. Aside from any deficiencies in the equipment, a major reason for the discrepancy is the asymmetry in the diffraction line profile from Si-Ge alloys. The diffraction lines from the alloys are considerably broader than those from the pure elements, as might be expected for alloys, and they are also significantly asymmetric. In the single-crystal method, it is customary to take as the diffraction angle the value midway between the half-intensity points. Because of the asymmetry, this does not correspond to the angle for peak intensity. Because of the uncertainties arising from asymmetry, we used compositions derived from single-crystal lattice-parameter measurements only for qualitative indications.

Separate determinations of lattice constant were also made using the powder method for a few of the samples. In this case, a Debye-Scherrer 114.7-mm camera was used, with the lattice constant determined by graphical extrapolation using the Nelson-Riley error function and six back-reflection lines due to Cu K_{α} radiation. It is conventional to use the peak positions of the diffraction lines in the powder pattern analysis, and, in those cases where the results were compared with those from other methods of determining composition, the powder results were in agreement. Measured lattice constants were converted to composition according to the calibrations of Dismukes, Ekstrom, and Paff.[2]

The broadening and asymmetry of the X-ray-diffraction lines are certainly associated with the alloy nature of the material. We cannot assess how much of this behavior is caused by non-uniformity of composition and how much would be present in an ideally uniform alloy. In a typical X-ray topograph of a Si-Ge sample, the light and dark bands are

most likely due to minute variations in composition, which correspond to the striations that normally appear in Czochralski-grown crystals because of the rotation of the crystal in a nonsymmetric thermal field. These striations come about because of changes in the solute distribution coefficient that occur in response to microscopic growth rate variations in the nonsymmetric thermal field. In Figure 4, only part of the wafer is in the Bragg condition because it was polished on only one side and is therefore warped; however, the striations can be clearly seen.

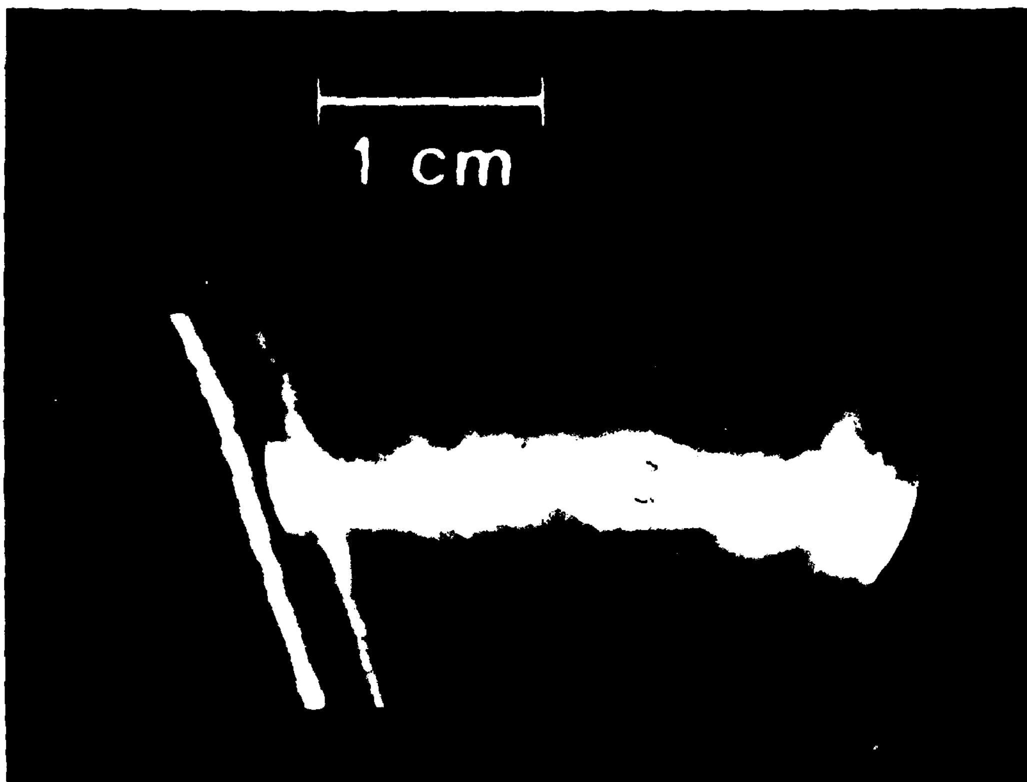

Figure 4. X-ray topograph of Si-Ge crystal, showing rotational striations caused by small variations in composition.

SECTION 6

OPTICAL AND ELECTRICAL MEASUREMENTS

A. INFRARED ABSORPTION MEASUREMENTS

We measured the infrared absorption near the band edge at room temperature for several Czochralski-grown Si-Ge samples of different compositions with a carefully calibrated and adjusted Cary spectrophotometer. The absorption coefficient α was determined from the expressions for transmission T and reflectivity R:

$$T = \frac{(1 - R)^2}{e^{\alpha d} - R^2 e^{-\alpha d}} \qquad (1)$$

$$R = \frac{(n - 1)^2}{(n + 1)^2} \quad , \qquad (2)$$

where d is the sample thickness, and n, the refractive index, is estimated from the value of transmission in the long-wavelength constant-transmission region beyond the band edge.

For all the samples studied, the square root of the absorption coefficient is expected to be a linear function of photon energy near 1.06 μm wavelength. Figure 5 shows that this expectation is realized. The curves of $\sqrt{\alpha}$ versus $h\nu$ for 10.9% and 11.3% alloys do not have the expected relative position at low values of α, although the discrepancy is small and apparently disappears at the highest α values we studied. Figure 6 shows the decrease in band edge (arbitrarily taken at $\alpha = 36\ cm^{-1}$) with increasing Ge content. The expected value of the absorption coefficient for $Si_{0.9}Ge_{0.1}$ at 1.06 μm is about 50 cm^{-1}.

B. HALL ANALYSIS

Measurements of Hall effect versus temperature were made on samples from three undoped crystals of Si-Ge and from two In-doped crystals of Si-Ge. Analysis of the data gives firm evidence that each configuration

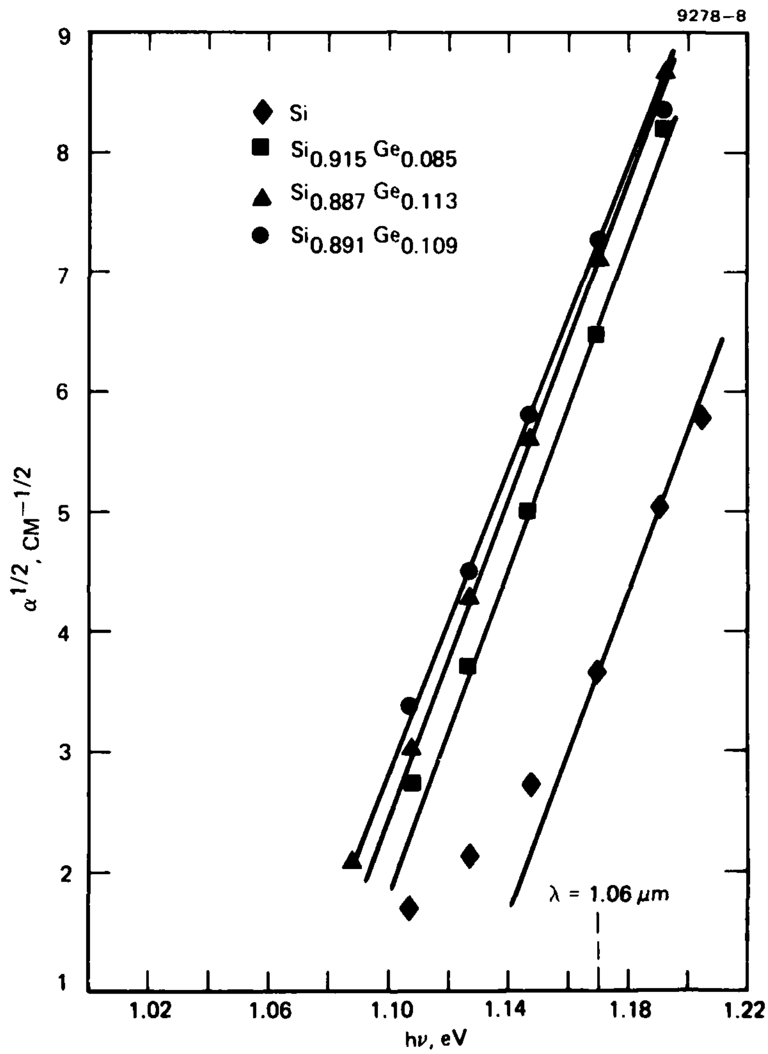

Figure 5. Dependence of absorption coefficient on photon energy at 292°K for Si-Ge alloys and Si.

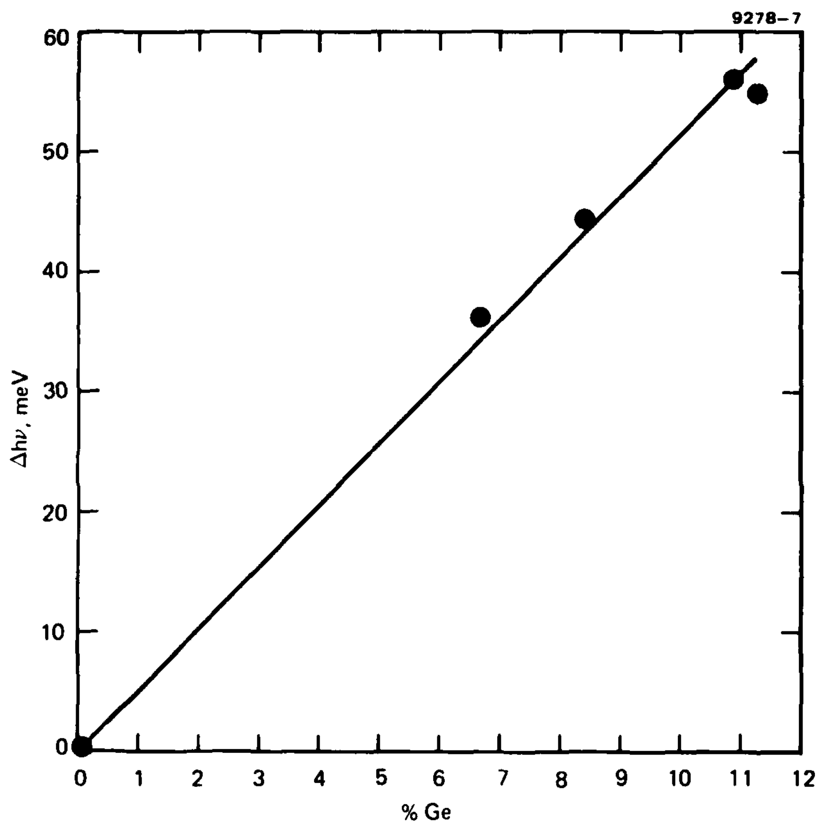

Figure 6. Shift in band edge (α = 36 cm^{-1}) versus composition.

of a boron impurity (e.g., the number of Ge and Si atoms occupying the four nearest-neighbor sites) gives rise to a different, relatively sharp, energy level as opposed to a continuous distribution of energy levels. The analysis also strongly suggests that the same phenomenon occurs for an indium impurity.

1. Method

The results were analyzed by fitting carrier concentration versus temperature to the charge-balance equations

$$p + N_D = \sum_i \frac{(N_A)_i}{1 + \frac{pg_i}{N_V} e^{E_i/kT}} \qquad (3)$$

using a nonlinear least-squares technique. Here, N_V is the valence band effective density of states; N_D is the total compensating donor concentration; and $(N_A)_i$, $g_i \equiv 4$, and E_i are the concentration, degeneracy, and ionization energy, respectively, for the ith acceptor. The sum in Eq. 3 is over all acceptors. For measurements taken over a finite temperature range, several simplifications occur. First, those acceptor levels that are deep enough so that they remain neutral at the highest temperature attained make no contribution to the sum. Second, those shallowest levels that are sufficiently overcompensated are always fully ionized and contribute just a constant $(N_A)_i$ to the sum. Since the fitting procedure cannot distinguish between constants, which get lumped with N_D, only a net compensation $N'_D = N_D - \sum_i (N_A)_i$ is determined (the sum in this case being over overcompensated shallow acceptors only). Third, the low temperature slope will be dominated by the shallowest undercompensated acceptor level. The free-carrier concentration p is related to the measured Hall coefficient R_H by

$$p = \frac{r}{eR_H} \quad , \qquad (4)$$

where r is the scattering factor.

In analyzing the data, several approximations were made necessary by lack of information. One such approximation is that r 1. Because r is a function of T, this assumption distorts the shape of $p(T)$ and leads to errors in the analysis. This effect is most clearly seen in the apparent increase in p at temperatures above $\sim$150°K in lightly doped Si:B and Si:Ge:B samples (for example, see Figure 7). This apparent increase in p reflects the large temperature dependence of r in this temperature range.[3] Analysis of the data for such samples was restricted to $T \lesssim 100$°K to avoid this effect. In the analysis of In-doped Si and Si-Ge, this large temperature dependence of r for $T \gtrsim 150$°K also leads to an overestimate of the indium ionization energy and concentration.[4] The use of the data in this temperature range cannot be avoided because of the relatively large value of E_{In} and the fact that the behavior of $p(T)$ at lower temperatures is dominated by undercompensated, shallower acceptors (B and X[5,6]).

The use of $N_V(T)$ for pure Si in the analysis of the data for Si-Ge is another approximation that was necessary since no data on the hole effective masses in Si-rich Si:Ge alloys are available.

The use of these approximations clearly introduces systematic errors with difficult to assess magnitudes into the densities and energies obtained from the Hall analysis. The effect of these approximations on relative changes in these quantities should introduce much smaller errors, since we expect that the systematic errors change relatively slowly. For the same reason, the presence of these errors should not obscure major features of the changes that take place as the Ge content is varied.

2. Results

The results of analyzing the Hall data are summarized in Table 3. All samples, whether doped with In or not, were dominated by boron at low temperatures, indicating that the boron was undercompensated. Two distinct energy levels — 0.042 and 0.035 eV — were observed for

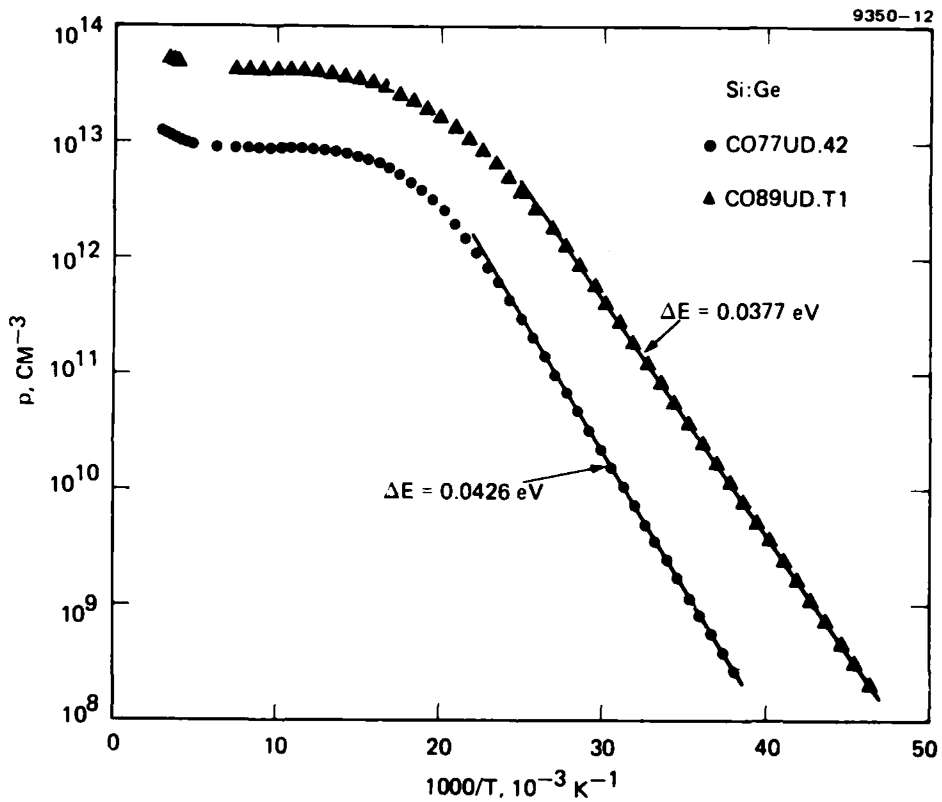

Figure 7. Carrier concentration versus temperature for Si:Ge:B showing explicit appearance of both of the observed energy levels depending on the degree of compensation.

Table 3. Si:Ge Hall Analysis Results

Parameter	Crystal Sample						
	C077UD.42	C089UD.T1	C092UD.T3	C093In.61	C110In.A2		C110In.T6
					SOLN.1	SOLN.2	
$(N_{In})_0$, cm^{-3}	--	--	--	2.5×10^{16}	4.8×10^{16}	3.9×10^{16}	4.8×10^{16}
$(E_{In})_0$, eV	--	--	--	0.125	0.135	0.141	0.134
$(N_{In})_1$, cm^{-3}	--	--	--	(average of k=0 and k=1)	1.1×10^{16}	2.1×10^{16}	1.0×10^{16}
$(E_{In})_1$, eV	--	--	--		0.107	0.114	0.105
N_{In}, cm^{-3}	--	--	--	2.5×10^{16}	6.0×10^{16}	6.4×10^{16}	5.9×10^{16}
N_X, cm^{-3}	--	--	--	--	2.2×10^{14}	4.8×10^{14}	1.9×10^{14}
E_X, eV	--	--	--	--	0.075	0.081	0.064
$(N_B)_0$, cm^{-3}	2.2×10^{13}	3.6×10^{13}	6.9×10^{14}	3.1×10^{15}	2.3×10^{14}	1.1×10^{14}	3.0×10^{14}
$(E_B)_0$, eV	0.0426	0.0412	0.0415	0.0408	-0.041-[b]	-0.041-[b]	0.0421
$(N_B)_1$, cm^{-3}	O.C.[a]	1.8×10^{13}	2.5×10^{14}	1.6×10^{15}	O.C.[a]	O.C.	O.C.
$(E_B)_1$, eV		0.0351	0.0346	0.0325			
N_B, cm^{-3}	3.6×10^{13}	5.7×10^{13}	9.8×10^{14}	5.0×10^{15}	3.6×10^{14}	1.7×10^{14}	4.8×10^{14}
N_D', cm^{-3}	1.4×10^{13}	1.3×10^{13}	1.6×10^{14}	2.1×10^{14}	2.2×10^{14}	9.8×10^{13}	2.1×10^{14}
N_D, cm^{-3}	2.8×10^{13}	1.7×10^{13}	1.9×10^{14}	5.3×10^{14}	3.5×10^{14}	1.6×10^{14}	3.9×10^{14}
rms err, %	1.8	0.9	0.8	1.0	0.34	0.36	0.9
Ge content from In ratio, %	--	--	--	--	5.3	11.8	5.1
B ratio, %	--	11.2	8.4	11.3	--	--	--
Microprobe, %	11.15						
Powder X-ray, %	11.3			10.4			10.9
Density, %	11.3	11.3	9.2				

[a]O.C. overcompensated, not observed.
[b]Value of parameter fixed during analysis.
Numerical subscripts denote the number of nearest-neighbor sites occupied by Ge.

6955

boron.* Both levels appear explicitly in the behavior of C089UD.T1, C092UD.T3, and C093In.61,† with the shallower 0.035-eV level dominating the low-temperature slope. The other three samples have a sufficiently large donor concentration so that the shallowest boron level is over-compensated and the deeper 0.042-eV level dominates the low-temperature slope. This is shown in Figure 6, where values of p(T) for C077UD.42 and C089UD.T1 are compared.

The necessity for including two acceptor levels for boron in the analysis is seen most clearly in the data for C093In.61. Table 4 compares the effects of assuming either one or two levels for boron on the analyses of the data for this sample. Both the rms and the maximum error of the one-boron-acceptor-level fit are unacceptably large and far worse than those for the two-boron-acceptor-level fit. The calculated p(T) curves for the two solutions given in Table 4 are shown in Figure 8 in comparison with the measured data. The lack of agreement between the shape of the measured p(T) and that of the fit obtained with the assumption of only one boron acceptor level is clearly evident. Also shown are the p(T) curves that would be observed if each of the two boron levels were present separately. Although these two curves add only approximately to the two-boron-acceptor-level fit, they do show the relative contribution of the two levels to p(T).

Our interpretation of the existence of these two discrete levels for the boron acceptor leads to the following model. The energy level of a given boron acceptor center is mostly determined by its four nearest neighbors. Thus, there should actually be five distinct energy levels for boron (or any other substitutional acceptor) depending on whether

---

*The slightly smaller values of the B energy levels observed for C093In.61 are probably significant, with the lowering of the levels being caused by the large concentrations of boron and donors.

†The sample numbering terminology is as follows: the first four characters are the crystal designation, the next two characters are either UD for undoped or In for indium doped, and the two characters after the decimal point are a slice and a sample designation, respectively.

Table 4. Analysis of Hall Data for C093In.61 Assuming One or Two Levels for Boron

Parameter	One B Level	Two B Levels
N_{In}, cm^{-3}	2.5×10^{16}	2.5×10^{16}
E_{In}, eV	0.121	0.126
$(N_B)_0$, cm^{-3}	--	3.1×10^{15}
$(E_B)_0$, eV	--	0.0408
$(N_B)_1$, cm^{-3}	3.6×10^{15}	1.6×10^{15}
$(E_B)_1$, eV	0.0328	0.0325
N_D', cm^{-3}	4.0×10^{14}	2.1×10^{14}
RMS error, %	6.7	1.0
Maximum error, %	26.8	2.0

6955

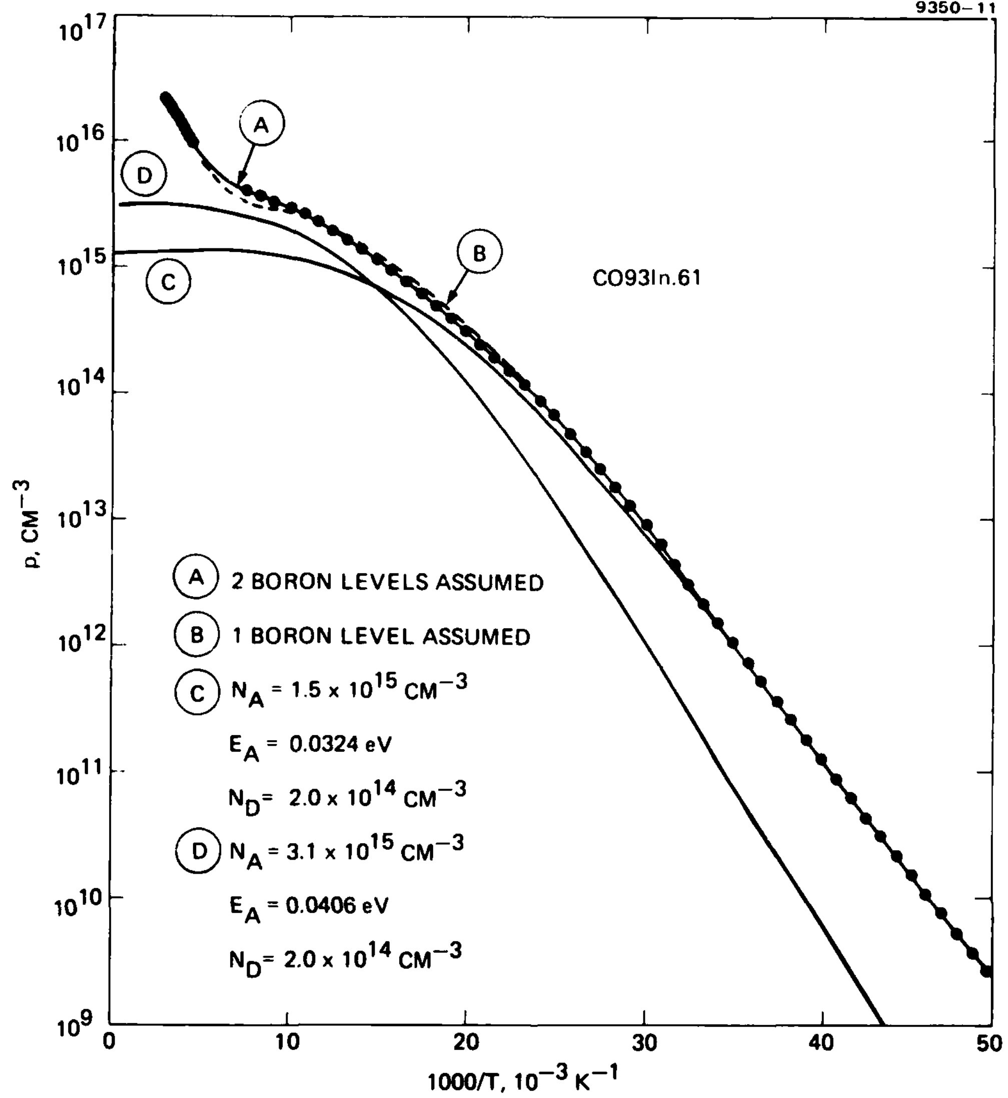

Figure 8. Carrier concentration versus temperature for Si:Ge:B.*

---

*The necessity of assuming two B levels is evident in the very poor fit to the data obtained when only one level is assumed. Curves C and D are the p(T) which would occur if each B level of the two-boron level fit existed by itself.

the number of nearest-neighbor sites occupied by Ge atoms was 0, 1, 2, 3, or 4. Non-nearest-neighbor sites affect the acceptor energy levels much less, probably leading to a relatively small broadening of the levels. Given this model, the concentrations of boron with each of these levels will be proportional to the probability of the corresponding occupation of the nearest-neighbor sites. Thus, if the presence of the boron does not affect the probability of a given site being occupied by a Si or a Ge atom, then the probabilities will be (1 - x) for Si and x for Ge in a $Si_{(1-x)}Ge_x$ alloy, and the probability of the four nearest-neighbor sites being occupied by k Ge atoms and (4 - k) Si atoms is given by the binomial distribution to be

$$P_k = \frac{4!}{(4 - k)!\ k!} (1 - x)^{4-k} x^k \quad . \tag{5}$$

A boron atom with all four nearest-neighbor sites occupied by Si atoms is clearly most similar to a boron atom in a pure Si lattice and would thus be associated with the deepest level. A boron atom with one nearest-neighbor site occupied by a Ge atom would have the next shallowest level, and so on.

Given a $Si_{1-x}Ge_x$ alloy with x = 0.113, such as determined for C077UD.42 and C089UD.T1 by means of density measurements, the expected probabilities are given in Table 5, along with values for several other values of x. Note that, in the range of Ge concentrations of interest, the values of P_k for $k \geq 2$ are very small. This is the reason that the shallower B levels which would be associated with the higher values of k are not observed, their concentrations

$$(N_B)_k \cong P_k N_B \tag{6}$$

being so small that they are overcompensated (the sum of their concentrations is less than the total donor concentration).

Table 5. Probability of a B Site in $Si_{(1-x)}Ge_x$: B Having k Ge Nearest Neighbors. Binomial Model $P_k = 4!/[(4-k)!\,k!]\,(1-x)^{(4-k)}\,x^k$

k	x = 0.05	x = 0.10	x = 0.113	x = 0.15
0	0.815	0.656	0.619	0.522
1	0.171	0.292	0.315	0.368
2	0.014	0.049	0.060	0.098
3	0.00048	0.0036	0.0051	0.011
4	0.0000063	0.00010	0.00016	0.00051

6955

Thus, we associate the 0.042- and 0.035-eV levels with B atoms having k = 0 and 1, respectively. If this is the case, then the Ge concentration is related to the ratio of the densities by

$$\frac{(N_B)_0}{(N_B)_1} = \frac{P_0}{P_1} = \frac{1-x}{4x} \quad , \qquad (7)$$

which may be solved for x to give

$$x = \left[1 + \frac{4(N_B)_0}{(N_B)_1}\right]^{-1} \quad . \qquad (8)$$

For the three samples for which both $(N_B)_0$ and $(N_B)_1$ are available, x has been calculated from Eq. 8 and given in Table 3 as "Ge content from: (B ratio)." The values of x determined in this manner are in good agreement with other measurements of x, considering that the error associated with this method probably is on the order of ±10%. This good agreement in the values of x is strong confirmation of the model.

Using this model, the total B and the compensating donor concentration can be calculated and are given in Table 3 as N_B and N_D, using x

from the B ratio when available and x from powder X ray otherwise.

One would expect similar behavior for In. The data for In, however, are not as easily interpretable as those for B. This is because under-compensated shallower levels dominate p(T) at lower temperatures, leaving only a relatively small range of the p(T) curve at higher temperatures dependent on In. For C093In.61, for example, only about a decade in p is dominated by In (see Figure 8) because of the high B concentration, and only a single, "average" In level can be inferred from the analysis of these data.* The situation is better for the samples from crystal C110In, where the boron concentration is much lower and is closely compensated. Figure 9 shows p(T) for C110In.T6. In this case, some 2 to 2-1/2 decades in p are dominated by In, and a best fit to the data is obtained when two In levels and an "X" level are provided for in addition to the B. Table 6 compares the results of providing for 2, 3, and 4 acceptor levels. The fit with two acceptor levels assumed is clearly unacceptable. Comparing the fits obtained with 3 or 4 acceptor levels, the results strongly suggest that 4 levels are necessary, particularly when the conclusion of the analysis of the boron level is taken into account, there being no physical reason that multiple levels reflecting the nearest-neighbor occupation should not exist for In if they exist for B.

Analysis of C110In.A2 is not as clear cut as two solutions with essentially equal measures of error are found. One solution parallels that found for C110In.T6 (let us call these type A solutions). The other differs slightly in the energies found for the In levels and by about a factor of two in $(N_{In})_1$ (let us call this a type B solution). No corresponding type B solution for C110In.T6 was found, but an exhaustive search is not possible.

---

*Although some points were missed because of equipment problems, the presence of these missed points would not significantly add information and the missing points were therefore not remeasured.

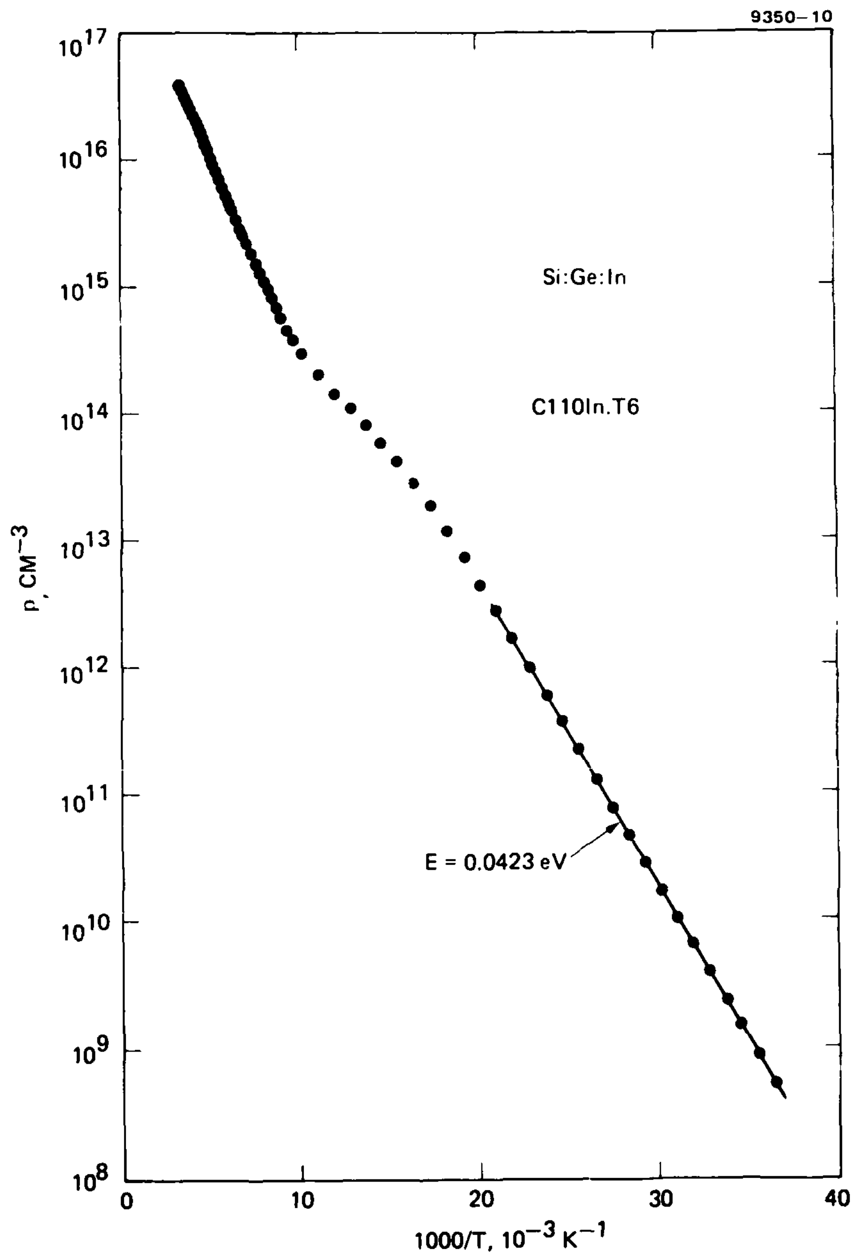

Figure 9. Carrier concentration versus temperature for Si:Ge:In showing the extent to which the data is dominated by undercompensated residual B.

Table 6. Analysis of Hall Data for C110In.T6

Parameter	Number of Acceptor Levels in Fit		
	2	3	4
$(N_{In})_0$, cm^{-3}	4.8×10^{16}	5.3×10^{16}	4.8×10^{16}
$(E_{In})_0$, eV	0.119	0.127	0.134
$(N_{In})_1$, cm^{-3}	--	--	1.0×10^{16}
$(E_{In})_1$, eV	--	--	0.105
N_X, cm^{-3}	--	2.1×10^{15}	1.9×10^{14}
E_X, eV	--	0.088	0.064
$(N_B)_0$, cm^{-3}	6.8×10^{14}	4.4×10^{14}	3.0×10^{14}
$(E_B)_0$, eV	0.0418	0.0422	0.0421
N_D', cm^{-3}	5.0×10^{14}	3.1×10^{14}	2.1×10^{14}
RMS error, %	5.1	1.3	0.9
Maximum error, %	12.3	3.1	2.4

6955

The Ge content inferred from

$$x = \left(1 + \frac{4(N_{In})_0}{(N_{In})_1}\right)^{-1} \quad (9)$$

(Eq. 8 rewritten for In) for these fits to C110In are given in Table 3 as "Ge content from : (In ratio)." The solutions that are common to C110In.A2 and C110In.T6 (type A) yield a Ge content about one-half of the expected value, while the type B solution yields a Ge content in good

agreement with the expected value. Multiple solutions probably exist because the model we are using is only approximate. The problem is worse for the determination of In parameters because the neglected temperature dependence of r is particularly strong for $T \geq 100°K$, where the information about the In level is contained. As a result, there are several possible interpretations of these results:

- The type-B solution is the proper one. It was not found for C110In.T6 because the least-squares fitting program, which takes a random starting point in parameter space and seeks a local minimum in the rms error, did not happen to choose a starting point that led to a type-B solution.

- The type-A solutions are the proper ones, and the values of x are correct, but must be interpreted properly. The large sizes of the In and Ge atoms reduce the probability that they will occupy nearest-neighbor sites in the lattice because of the large strain that would result. Thus, the relative occupation of nearest-neighbor sites around an In atom by Ge atoms is correctly given by Eq. 9 as $\sim$5%, but is not characteristic of the relative occupation of a random lattice site by a Ge atom.

- The type-A solutions are the proper ones, but the values are so distorted by the approximations of the analysis that the value of x inferred is in error by a factor of 2.

The first interpretation is possible but not very probable. Ten different random starting points were used; this is normally sufficient to uncover all possible solutions (local minima). The second interpretation is physically very reasonable, but it is not possible at present to decide whether it, the third interpretation, or some combination of the two is more valid.

As can be seen in Tables 3 and 6, a reasonable fit to Si-Ge:In data definitely requires the inclusion of an additional acceptor level whose energy lies in the range of 0.064 to 0.081 eV. This level corresponds to the "X" level found in Si:In, which has been determined to be caused by a defect consisting of a carbon-indium pair.[3,4] The scatter in E_X primarily occurs because only a small range of the data, lying between the In- and B-dominated regions, is sensitive to the presence of this

level, leading to a very broad minimum in the error surface for this parameter. The rather large values found for N_X and E_X in the three-acceptor fit shown in Table 6 most likely represent an average between X and some of the In states. Because of the small amount of information available in the data, the values for N_X and E_X represent an average of the "X" level states. Note that there are only four possible nearest-neighbor occupation states for the "X" level as this defect has only three nearest-neighbor sites available for occupation by a Si or Ge atom.

Our results for E_A versus Ge content are shown in Figure 10, along with our Hall results for E_B, E_X, and E_{In} in pure Si and the values for E_B and E_{In} reported by Morton et al.[7] There is good agreement between our measurements of $(E_B)_0$ and $(E_{In})_0$ and the results of Morton. The values of $(E_B)_1$ and $(E_{In})_1$ are significantly smaller than the k = 0 values, and we expect that the k = 1 values of E would vary with Ge content in the same manner as the k = 0 values of E, as indicated by the dashed lines in Figure 10. The point for E_X represents an average value and would lie between $(E_X)_0$ and $(E_X)_1$. The observed change from the value of E_X in pure Si seems reasonable when compared with the In and B data.

3. Mobility

Plots of Hall mobility versus temperature for the undoped crystals (Si:Ge:B) and the In-doped crystals (Si-Ge:In) are shown in Figures 11 and 12, respectively. In each case, $\mu_H(T)$ for a very pure Si sample and for Si samples of comparable doping are shown for comparison. The mobilities of the Si-Ge samples are significantly lower than those of the Si samples because of the additional scattering of carriers caused by the disorder of the alloy.

The mobility due to disorder scattering can be calculated approximately from

$$\frac{1}{\mu_{disorder}} = \frac{1}{\mu_{Si:Ge}} - \frac{1}{\mu_{Si}} \qquad (10)$$

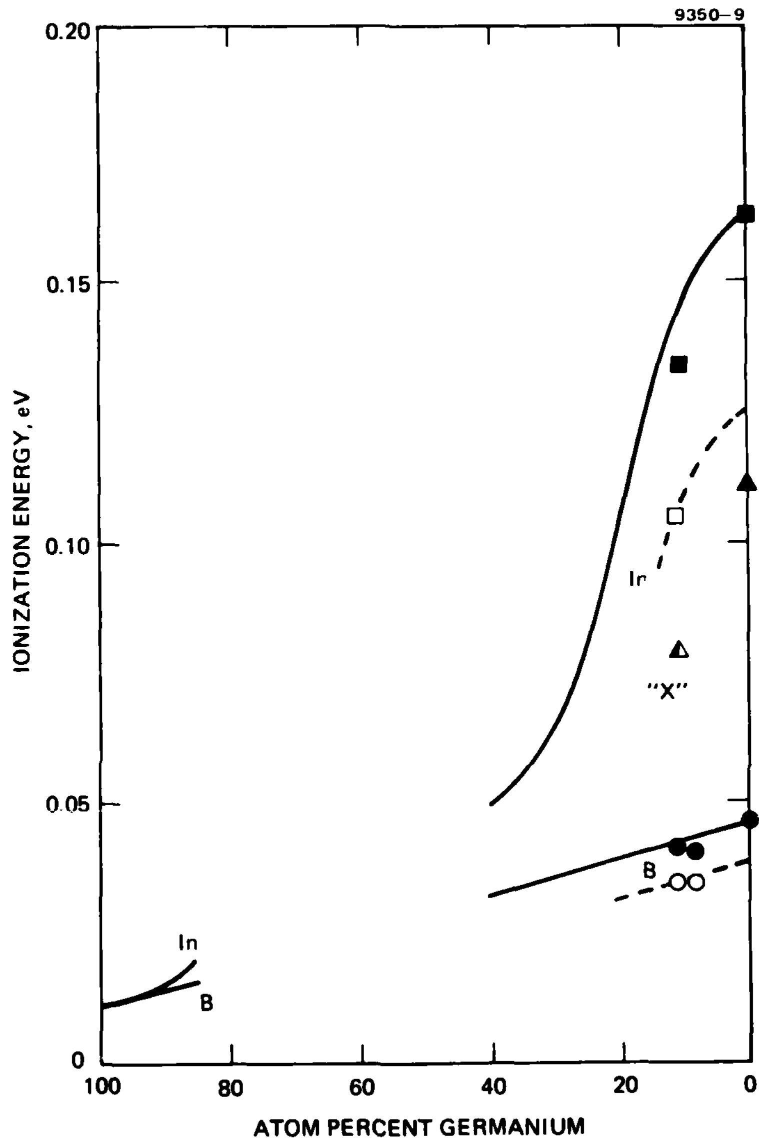

Figure 10. Observed ionization energies versus x in $Si_{(1-x)}Ge_x$.*

---

*Solid points are values for k = 0 (no Ge nearest-neighbors) and open points are values for k = 1 (one Ge nearest-neighbor). The half-shaded point for "X" level indicates that the value is an average k = 0 and k = 1 states. The points at x = 0 are from previous work at this laboratory.

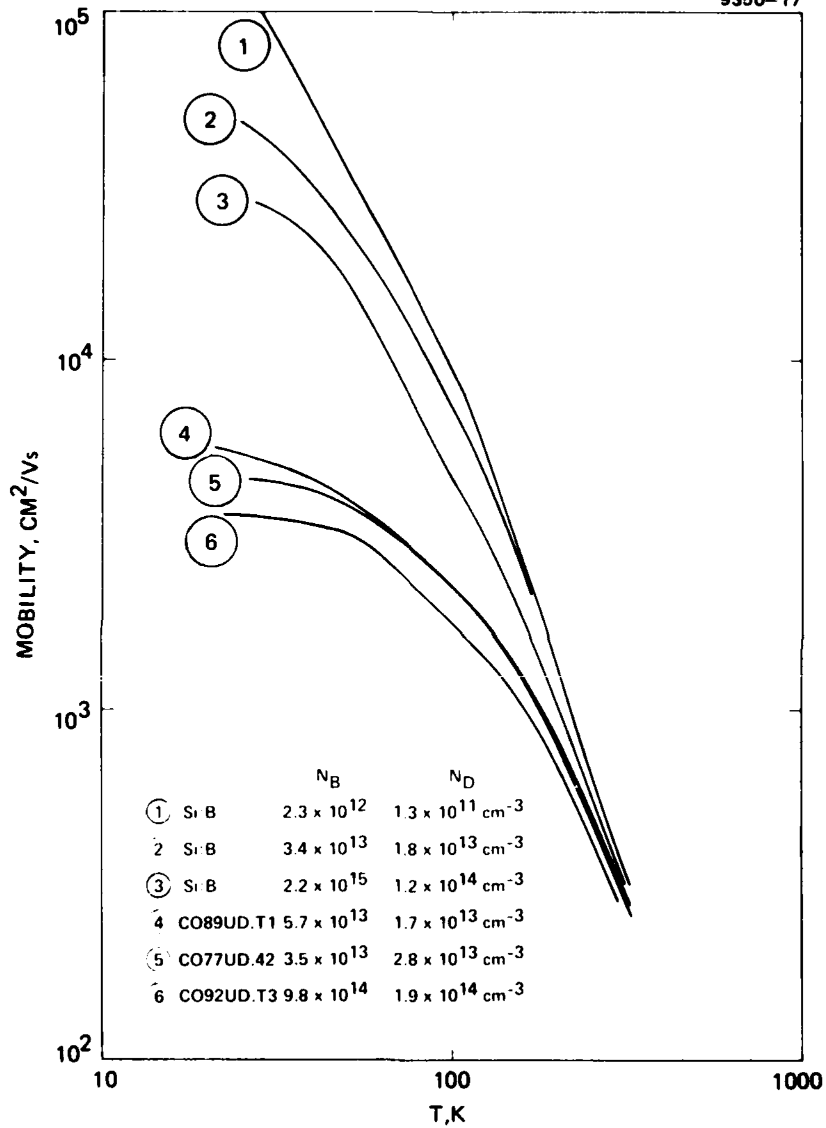

Figure 11. Mobility versus temperature for a number of Si:Ge and Si samples.

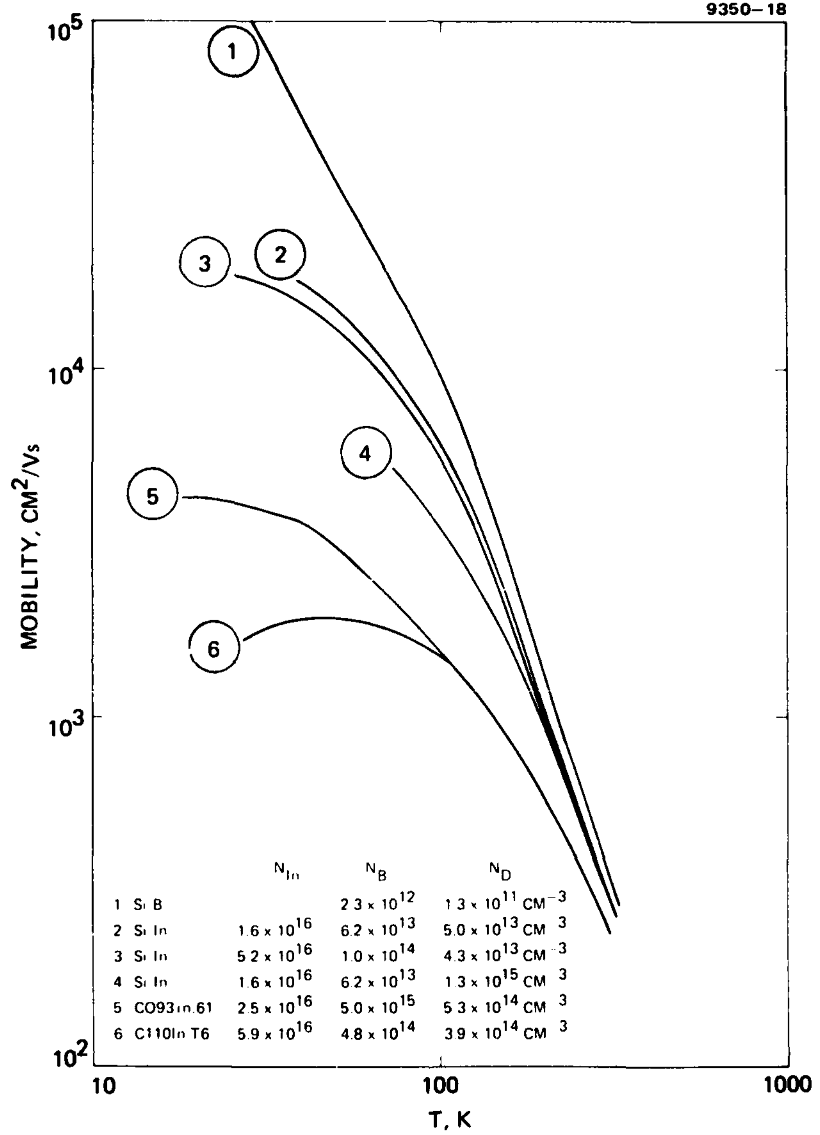

Figure 12. Mobility versus temperature for a number of In-doped Si:Ge and Si samples.

if all other scattering mechanisms are equivalent. The value of μ_{Si} for a given set of doping parameters corresponding to a particular Si-Ge sample may be estimated by interpolating the results for the silicon samples in Figures 11 and 12. The major contribution to scattering is ionized impurity scattering, neutral impurity scattering being small (compare curves 2 and 3 in Figure 12). Plotting $1/\mu$ versus $N_{ionized} = p + 2N_D$ at a given T yields a curve that may be used to interpolate the effects of ionized impurity scattering. An additional small correction for the effects of neutral impurity scattering may be made using the results of Baron, Young, and McGill.[8] This has been done for T = 60°K for comparison with the scattering lifetimes measured in Si-Ge at that temperature by Fink and Braunstein[9] using cyclotron resonance. Figure 13 compares their results, our data from this contract, and some earlier data of ours on samples of $Si_{0.933}Ge_{0.067}$:P and $Si_{0.926}Ge_{0.074}$:In. Given the approximate nature of the calculations, the agreement is very good.* Our evaluation of $\mu_{disorder}$ is also shown in Figure 14, where it is compared to the expected shape of the theoretical dependence of $\mu_{disorder}$ on x of[9]

$$\mu_{disorder} \propto \left[x(1 - x)\right]^{-1} . \qquad (11)$$

In this figure, the theoretical curve given by Eq. 11 has been arbitrarily normalized to pass through the data point for the Si-Ge:P sample. Again, given the approximate nature of the calculation to determine μ_{Si}, a reasonable fit to the theoretical shape is obtained.

Because of the unavoidable scattering caused by disorder, the mobility and thus the detector responsivity will be degraded in Si-Ge detectors. This effect is most noticeable at low temperatures where the mobility of Si devices is high and is most affected by the disorder scattering. At room temperature, the already much lower mobility of Si

*The point corresponding to curve 6 of Figure 12 is not shown since the lower mobility reflects the almost exact compensation of the boron and is an artifact of the measurement technique under such conditions.

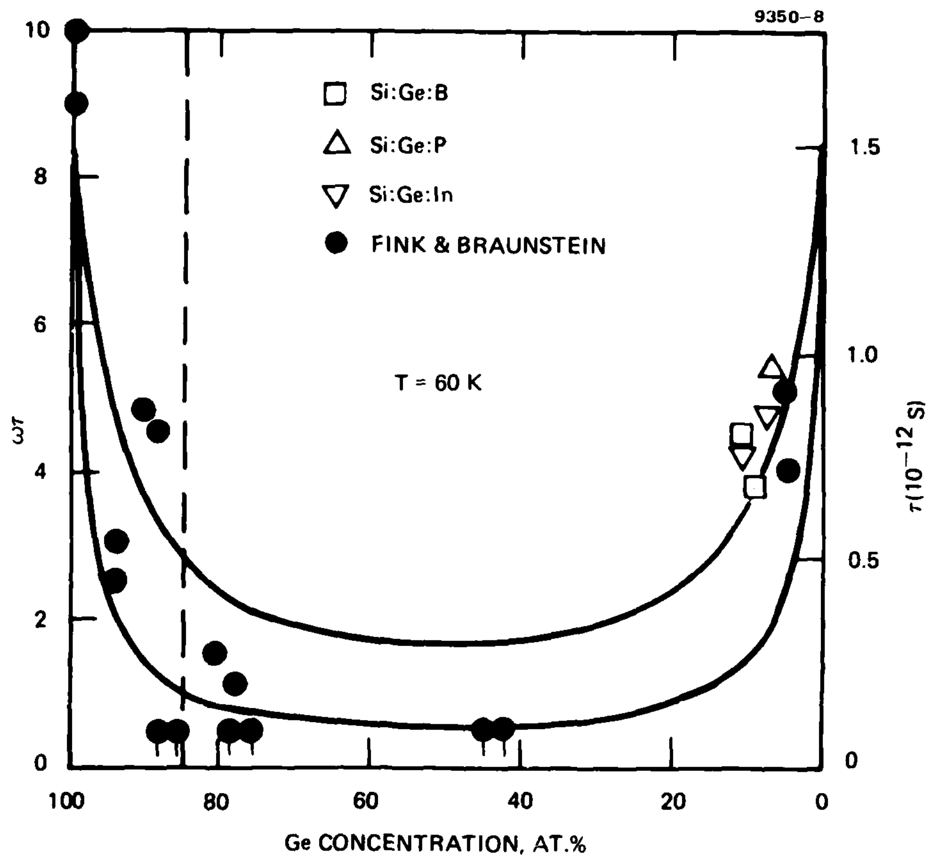

Figure 13. Comparison of disorder induced scattering lifetimes in Si:Ge.

results in a much smaller degradation in mobility, amounting to only 10 to 20% in p-type material. Of course, in a p-i-n structure where both electrons and holes contribute, the high mobility of the electrons will result in their mobility being decreased more than that of the holes.

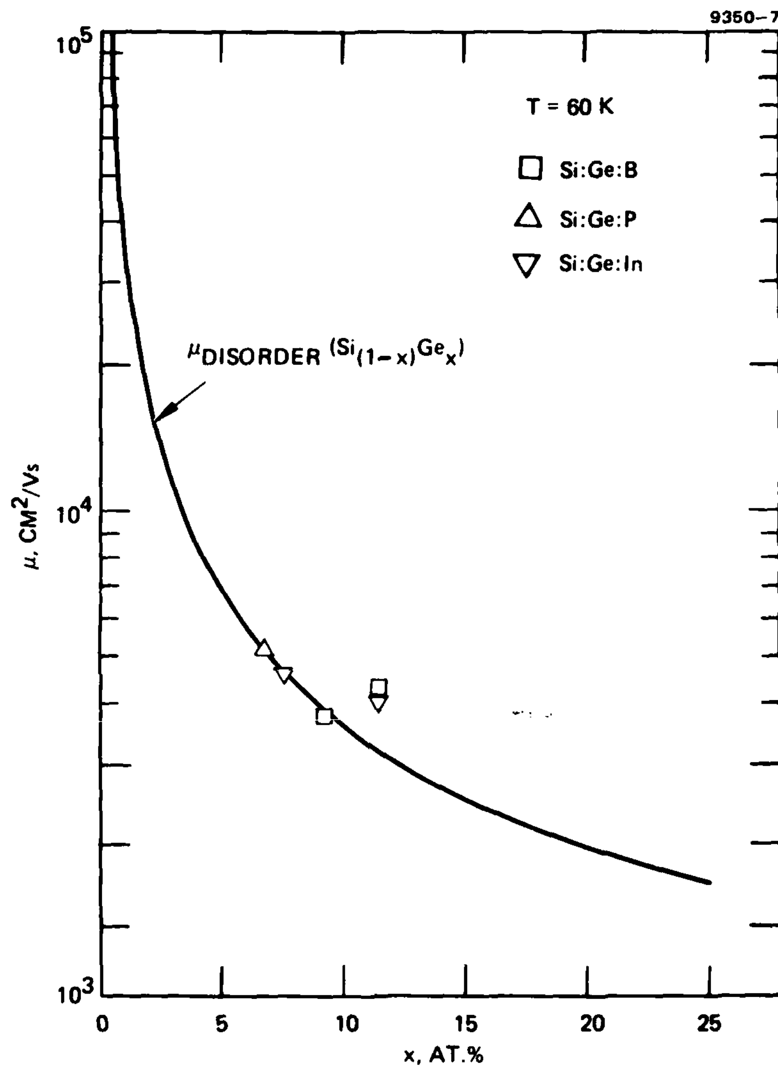

Figure 14. Comparison of $\mu_{disorder}$ versus x in $Si_{(1-x)}Ge_x$ to the theoretical expected shape.

C. NEAR-INFRARED SPECTRAL RESPONSE MEASUREMENTS

We fabricated $n^+\pi p^+$ structures from samples of undoped p-type Si-Ge crystal C077 and also from pure Si samples of the same resistivity in order to compare the relative intrinsic spectral response of Si-Ge to Si in the 0.6- to 1.3-μm range. Spectral measurements on these samples also allowed us to estimate the important material parameter of diffusion length in the Si-Ge.

Ion implantation of 10^{15} As/cm^2 at 50 keV provided the n^+ top layer, and an implant of 10^{15} B/cm^2 at 20 keV provided the ohmic back contact to these photosensitive diodes. A low-temperature anneal at 650°C for 1 hr activated the implants. Room-temperature Hall and resistivity measurements on the implanted layers in Si-Ge indicated 50% activation of the ion implant for the n^+ side and 5% activation for the p^+ layer. The latter is about what would be expected for a corresponding B implant in Si annealed at 650°C.

A mesa structure was etched on the n^+ side to define the junction and reduce leakage. Indium solder metalization was used on both the n^+ and p^+ sides. I-V measurements made at room temperature in the dark indicated quite acceptable diode characteristics for these devices.

The spectral measurements were made using a monochromatic light source chopped at 13 Hz. The ac photocurrent was monitored by using a current-sensitive preamplifier and lock-in amplifier set to the chopping frequency.

D. MINORITY-CARRIER DIFFUSION LENGTH

Spectral response was measured at several values of reverse bias as well as at $V_B = 0$ (short-circuit current). From these data, minority-carrier diffusion length can be determined.

The current in an illuminated p^+-π-n^+ detector is given by[10]

$$I = e\Phi_o A\left(1 - \frac{e^{-\alpha W}}{1 + \alpha L_n}\right) \qquad (12)$$

in the limit when the photogenerated current is much larger than the dark current, a condition that is satisfied in our experiment. In Eq. 12, Φ_o is the incident photon flux, A is the junction area, α is the absorption coefficient for electron-hole pair generation, W is the width of the depletion region, and L_n is the electron (minority-carrier) diffusion length in the π region. The contribution to the diffusion current in the very thin, heavily doped n^+ contact is negligible and has not been included in Eq. 12. In the limit when $\alpha W << 1$, Eq. 12 reduces to

$$I = e\alpha\Phi_o A(L_n + W) \tag{13}$$

and so a plot of I versus W would yield a straight line whose slope,

$$dI/dW = e\alpha\Phi_o A \quad , \tag{14}$$

and intercept,

$$I(0) = e\alpha\Phi_o AL_n \quad , \tag{15}$$

are enough to determine L_n from

$$L_n = \frac{I(0)}{dI/dW} \quad . \tag{16}$$

The width of the depletion layer is related to the applied bias, V_B, and the net doping, $(N_B - N_D)$, in the π layer by

$$W = \sqrt{\frac{2 \ (V_B + V_o)}{e(N_B - N_D)}} \quad . \tag{17}$$

The built-in junction potential, V_o, is given by

$$V_o = \left(\frac{kT}{e}\right) \ln \left[\frac{N^+ (N_B - N_D)}{n_i^2}\right] , \tag{18}$$

where N^+ is the doping in the n^+ layer, and n_i is the intrinsic carrier concentration.

Figure 15 shows plots of I versus W for spectral response data at several wavelengths taken on an n^+-π-p^+ structure using material from C077UD as the π layer. Each plot is indeed a straight line, and the values of L_n calculated from Eq. 16 for each wavelength are also shown in the figure. The values of L_n are quite consistent, yielding an average value of $L_n = 13.0 \pm 0.5$ µm. Similar data for Si:B of nearly equal doping are presented in Figure 16. Again, except for $\lambda = 1.09$ µm, the data fit straight lines reasonably well and yield consistent values of L_n with an average value of $L_n = 19.9 \pm 2.1$ µm. We do not yet understand why the data for $\lambda = 1.09$ µm give a much larger value for L_n, since the condition $\alpha W \ll 1$ is still well satisfied, the maximum value for αW being 0.014.

The diffusion length for the Si-Ge sample compares very favorably with that for the Si sample. We may also compare the minority-carrier lifetimes inferred from these values of L_n. Using $\mu_n = 1375$ cm^2/Vsec for Si, $\mu_o = 726$ cm^2/Vsec for Si-Ge*, and the relation

$$\tau_n = \frac{L_n^2}{D_n} , \tag{19}$$

where the diffusion constant is related to the mobility by $D_n = (kT/e)\mu_n$, the values obtained are $\tau_n = 90 \pm 3$ nsec for the Si/Ge sample and $\tau_n = 110 \pm 12$ nsec for the Si sample. Thus, the Si/Ge material is essentially equivalent to the Si material in lifetime when both are processed as described above.

---

*Calculated from Eq. 10 using $\mu_{Si} = 1375$ cm^2/Vsec and $\mu_{disorder} =$ 1540 cm^2/Vsec reported for $Si_{(1-x)}Ge_x$:P with x = 6.7 at.% at 297°K in our proposal for this contract.

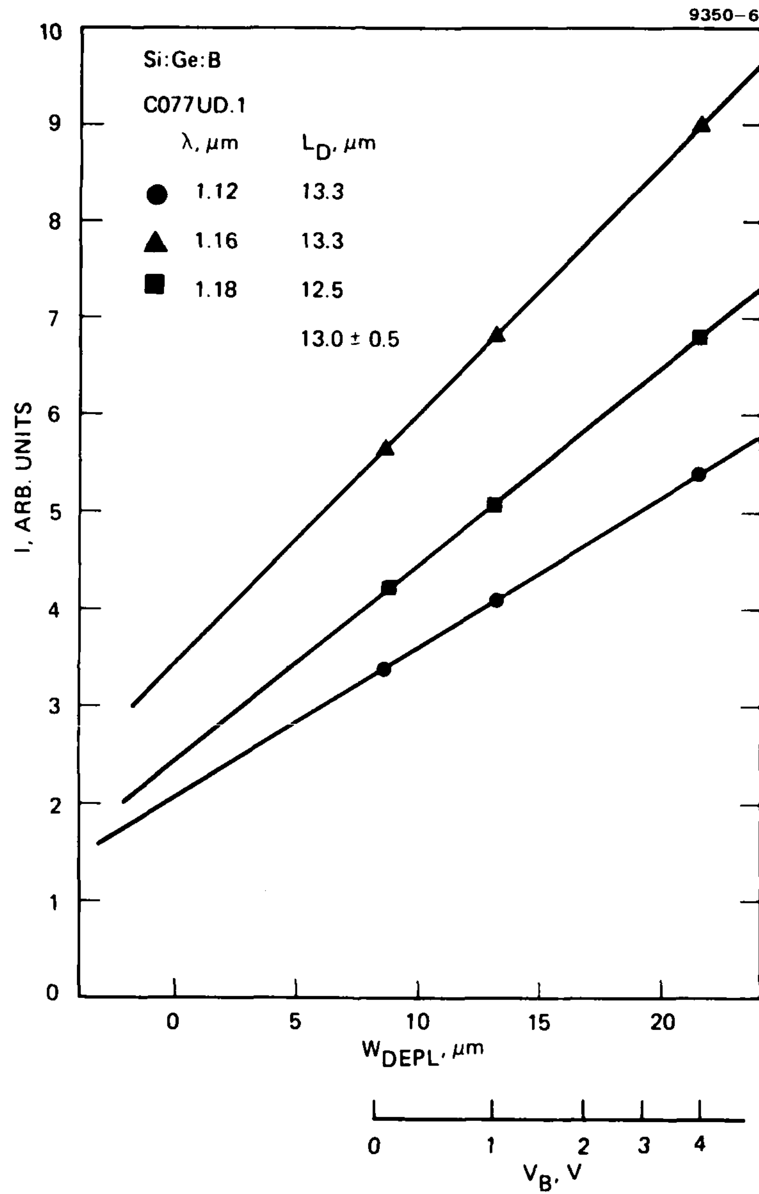

Figure 15. Photocurrent versus depletion layer width for Si:Ge $p^+\pi n^+$ structure.*

---

*Estimation of diffusion length from Eq. 16.

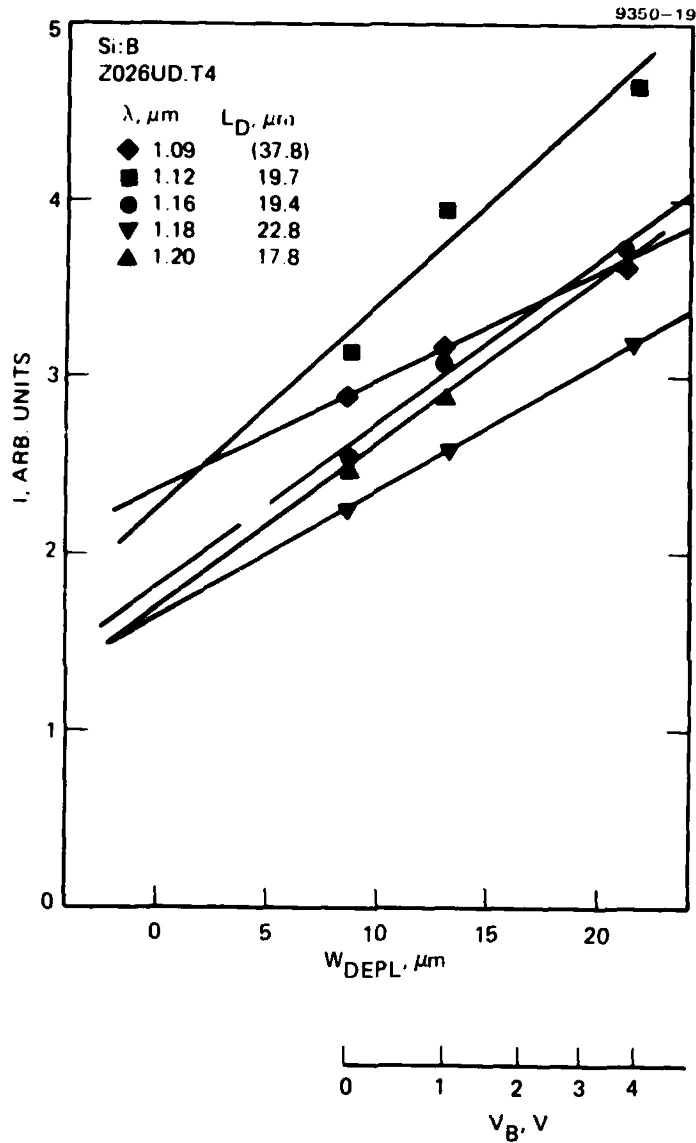

Figure 16. Photocurrent versus depletion layer width for Si $p^+ \pi n^+$ structure.*

*Estimation of diffusion length from Eq. 16.

E. SPECTRAL RESPONSE

Using the values of L_n determined above, it is possible to compare the spectral responses of Si and Si-Ge. This information is necessary since the quantity of interest, $\alpha(\lambda)$, is related to the photocurrent by Eq. 13, which, when solved for α, gives

$$\alpha = \frac{I}{e\Phi_o A(L_n + W)} \quad . \tag{20}$$

Since Φ_o and A are identical for the two measurements, the measured photocurrent must be scaled by $(L_n + W)$ to give a response proportional to α. This has been done in Figure 17 for the short-circuit photocurrent ($V_B = 0$), which corresponds to W = 8.6 μm for both devices. The results are somewhat puzzling. For $\lambda \gtrsim 1.2$ μm, the shift in the absorption edge is approximately as expected.[12] At $\lambda \simeq 1.2$ μm, there is a large jog in the Si-Ge data and a much smaller jog in the Si data. This effect is not understood, but may be an instrument problem. It is not a breakdown in the conditions which make $I \propto \alpha$, since αL_n and αW remain $\ll 1$ to much shorter wavelengths. Further work is needed to clarify this result.

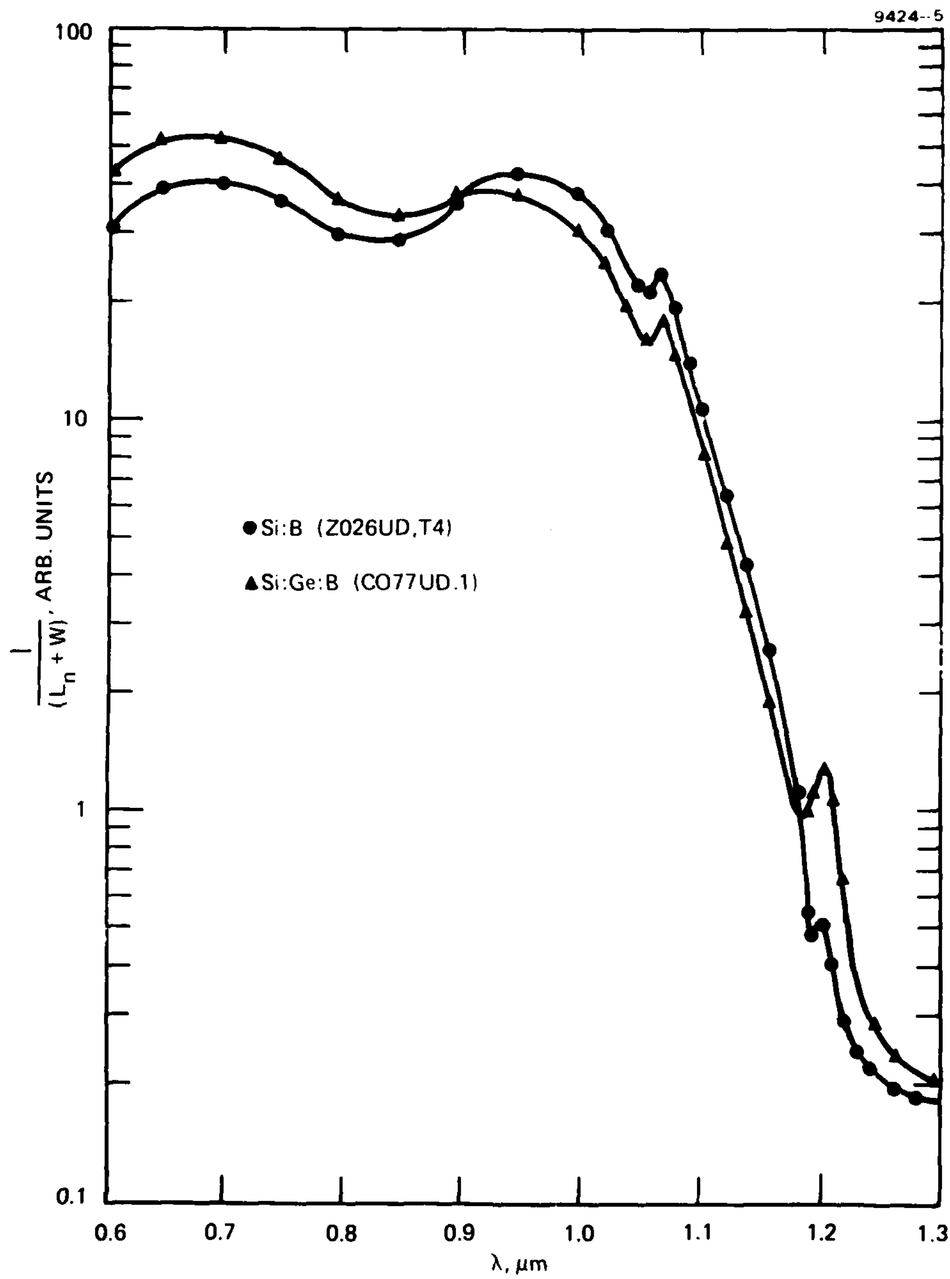

Figure 17. Relative photocurrent versus wavelength for Si and Si:Ge $p^+ \pi n^+$ structures.*

---

*Scaled to remove dependence on $(L_n + W)$.

SECTION 7

CONCLUSIONS AND RECOMMENDATIONS

During this two-year program we achieved the following results:

- Czochralski growth of $Si_{1-x}Ge_x$ on Si seed with $x > 0.1$
- P-type resistivity as high as 1700 Ω-cm
- N_B as low as 5×10^{13} cm^{-3} in Czochralski crystals
- $N_{In} = 5 \times 10^{16}$ cm^{-3}
- E_{In} as low as 0.107 eV
- Absorption coefficient at 1.06 μm up to 53 cm^{-1} (for Si it is 14 cm^{-1})
- Demonstration of nearest-neighbor influence on acceptor levels; the number of Ge neighbors is the strongest influence on acceptor energy levels in Si-Ge.

Despite these interesting results, we did not succeed in developing a method for producing Si-Ge alloy material suitable for use in detectors either at 1.06 μm or in the 8- to 12-μm range. For the 1.06-μm application, we produced crystalline material with suitably enhanced 1.06-μm absorption; however, the resistivity of this material was not high enough to allow an adequately long depletion region in a p-i-n detector. It does not appear that any Czochralski-type growth method can result in Si-Ge alloys with high enough resistivity, because of contamination from the crucible and heaters. Although we showed that Si-Ge alloy crystals can be grown by a crucible-free method, they had at best too low a Ge content and were axially nonuniform because of the depletion of Ge during growth. We are not at all confident that this crucible-free method can be extended, even with a great deal of growth equipment development, to provide uniform crystals of $Si_{0.9}Ge_{0.1}$. For the 8- to 12-μm range, we did demonstrate the presence of an In level with a binding energy of 0.107 eV, close to ideal for this spectral region. But since the material we made did not have the proper concentration of compensating donors, it was boron-dominated and could not operate at the temperature

appropriate to the 0.107-eV In level. Although this drawback could be overcome with additional work, a more fundamental difficulty is that only part of the In (about 29%) is in a crystalline site with the 0.107 eV value for the level. Most of the rest of the In exhibits a deeper level, and a small fraction presumably has still shallower levels. Although the shallower levels could be compensated by the careful addition of phosphorus donors, the inevitable presence of the deeper levels would necessitate having total concentrations of In much larger than those required in Si:In detectors, which are already difficult to achieve along with good crystallinity.

For these reasons, even though we did demonstrate tuning of the bandgap and of the In acceptor level by varying the Ge content, we do not recommend further work aimed at producing Si-Ge alloy crystals for infrared detector applications. We believe that the simultaneous constraints on composition, composition uniformity, resistivity or purity, crystallinity, and doping and compensating impurity concentrations make it unlikely that suitable detector materials could ever be produced except perhaps in very low yield in the laboratory. On the other hand, Si-Ge alloys constitute a unique system for the study of certain kinds of semiconductor interactions, including the local-environment-dependent impurity levels revealed in our work, and we hope that fundamental studies of this kind will continue in our own and other laboratories.

REFERENCES

1. H. Winston and H. Kimura, "Silicon-Germanium Alloys for Infrared Detectors," Interim Report, 15 August 1977 through 14 August 1978, AFML-TR-79-4043, April, 1979.

2. J.P. Dismukes, L. Ekstrom, and R.J. Paff, J. Phys. Chem. 68, 3021 (1964).

3. R. Baron, M.H. Young, J.K. Neeland, and O.J. Marsh, Proc. of the 3rd International Symposium on Silicon Materials Science and Technology, Edited by H.R. Hugg and E. Sirtl (The Electrochemical Society, 1977) p. 367.

4. R. Baron, M.H. Young, J.P. Baukus, O.J. Marsh, and M.J. Sheets, Proc. of the IRIS Specialty Group on Infrared Detectors, 1977 (Infrared Information and Analysis Center, Ann Arbor, 1977) Vol. I, p. 23.

5. R. Baron, M.H. Young, J.K. Neeland, and O.J. Marsh, Appl. Phys. Lett. 30, 594 (1977).

6. R. Baron, J.P. Baukus, S.D. Allen, T.C. McGill, M.H. Young, H. Kimura, H.V. Winston, and O.J. Marsh, Appl. Phys. Lett. 34, 257 (1979).

7. G.A. Morton, M.L. Schultz, and W.E. Harty, RCA Review 20, 599 (1959).

8. R. Baron, M.H. Young, and T.C. McGill, Proc. of the 13th Conf. of Semicond., edited by L.G. Fumi (Tipographia Marves, Rome, 1977) p. 1158.

9. D. Fink and R. Braunstein, Phys. Stat. Sol. (b) 73, 361 (1976).

10. S.M. Sze, "Physics of Semiconductor Devices," (John Wiley & Sons, Inc., N.Y., N.Y., 1969) p. 665.

11. Hughes Research Laboratories, Research on Silicon Germanium Alloys for Infrared Detectors, Part 2, Technical Proposal, 77M-0173/D9892, February 1977, p. 25.

12. R. Braunstein, A.R. Moore, and F. Herman, Phys. Rev. 109, 695 (1958).

*U.S.Government Printing Office: 1980 — 657-084/51